



Effect of surface tension gradients on coalescence dynamics of two unequal-sized drops

Swati Singh ^{*} and Arun K. Saha [†]

Department of Mechanical Engineering, Indian Institute of Technology Kanpur, Kanpur 208016, India



(Received 9 December 2022; accepted 28 April 2023; published 24 May 2023)

The coalescence dynamics of two unequal-sized drops made of miscible but distinct liquids has been numerically simulated using the coupled level set and volume of fluid method. Effect of the surface tension ratio of two liquid drops, the Ohnesorge number and the diameter ratio of two parent drops on three different pinch-off regimes, namely, first-stage, second-stage, and no pinch-off, are explored. The result shows that the coalescence process of two miscible liquid drops exhibits a nonmonotonic behavior of partial coalescence from appearance to disappearance and then reappearance with decreasing surface tension ratio. The strong lifting force of the intense Marangoni flow causes the reappearance of partial coalescence at higher surface tension difference between two drops. When the Ohnesorge number increases, high viscous forces restrict the propagation of Marangoni flow and do not favor the pinch-off, even in the presence of a significant surface tension difference. The generation of secondary drops at a considerable surface tension difference is also prevented for small parent drop size ratio. A regime map for the distinct coalescence outcomes is presented for different surface tension ratios. The critical surface tension ratio necessary for partial coalescence to occur grows monotonically as the Ohnesorge number increases. In our simulation, the minimum value of critical surface tension ratio needed for partial coalescence to take place is 0.94 at small values of the Ohnesorge number and the Bond number.

DOI: [10.1103/PhysRevFluids.8.053604](https://doi.org/10.1103/PhysRevFluids.8.053604)

I. INTRODUCTION

The coalescence of a drop on a flat liquid interface or between two drops has been seen in a wide range of natural and industrial systems [1–3], including raindrop/cloud formation [4], spray atomization [5], emulsion coarsening [6], and microfluidic devices [7]. When a drop makes contact with an interface, a significant portion of surface energy is released, which is then transferred to the kinetic energy, causing significant oscillation of the interface [8]. There could be two very different outcomes: complete coalescence, in which the drop merges completely with the bulk liquid, or partial coalescence, in which only a portion of the drop liquid merges with the bulk liquid, leaving a secondary drop. The generated secondary drop may repeat the partial coalescence process numerous times, resulting in an interesting self-similar coalescence cascade [9,10]. The first complete experimental work on the coalescence process was done by Charles and Mason [11] almost half a century ago, and since then, researchers have been working to gain a deeper understanding of this phenomenon. The introduction of high-speed cameras and strong numerical tools in recent years has also provided a new opportunity to analyze the process in greater depth [9].

*swatishi@iitk.ac.in

[†]Corresponding author: aksaha@iitk.ac.in

When the surrounding fluid separating the drop and the interface starts to drain out, the coalescence process begins [10]. The drainage of fluid from the drop forms a thin film between the drop and the interface [12,13]. As the thickness of thin film reduces, van der Waals force comes into play, triggering coalescence by generating a hole that expands rapidly due to capillarity [14]. Several researchers have done extensive research on the expansion of a hole [15–17]. They concluded that the interface dynamics are completely governed by the balance of viscous and capillary forces and found that the Ohnesorge number ($Oh = \mu/\sqrt{\rho D\sigma}$), i.e., defined as the ratio of viscous to capillary forces, is the best parameter to control this phenomenon. Here D represents the drop diameter, ρ and μ represent the density and viscosity of drop liquid, respectively, and σ is the surface tension. Based on the range of Oh , three different coalescence regimes have been observed: (a) viscous-capillary regime ($Oh > 1$), where interface dynamics is governed by viscous forces; (b) inertio-capillary regime ($Oh \ll 1$), where surface tension forces dominate the interface dynamics and the flow in this regime behaves as a nearly inviscid one; and (c) for intermediate Ohnesorge number, an intermediate regime connecting the viscous-capillary and inertio-capillary regimes [18].

For intermediate range of Oh , Thoroddsen and Takehara [9] examined the partial coalescence process and observed the well-known coalescence cascade, in which secondary drops are generated up to six successful consecutive coalescence steps before totally merged into the bulk liquid. For low viscosity liquids, Chen *et al.* [19] experimentally observed the partial coalescence process for a certain range of drop diameters. They further classified this range into three subregimes—the inertio-capillary, the viscous, and the gravitational regime—and found that the partial coalescence happens mainly in the inertio-capillary regime. Blanchette and Bigioni [10] explained the mechanism of secondary drop generation through their experimental and numerical works. They suggested that the secondary drop pinch-off process is completely governed by the convergence of the capillary waves at the apex of drop rather than the previously known Rayleigh plateau instability. Gilet *et al.* [20] reported that the phenomenon of partial coalescence depend mainly on the Bond number, the Ohnesorge numbers, and the relative density difference of two liquids. They found that the Bond number and Ohnesorge number should be below a critical value for the occurrence of partial coalescence and also reported the value of critical Oh to be 0.026 ± 0.003 for low Bond numbers.

The numerical work of Ray *et al.* [21] also revealed that the transition between partial and complete coalescence is mainly determined by the competition between horizontal (i.e., capillary pull which assists in the neck pinch-off) and vertical (i.e., inertioviscous which assists in the complete coalescence) rate of momentum. The pinch-off mechanism between two different-sized drops has been studied by Zhang *et al.* [22]. They described that the critical diameter ratio of two drops above which a secondary drop formed can be as small as 1.55 and the critical ratio increases as the Ohnesorge number increases. A new type of pinch-off known as a second-stage pinch-off also reported by several authors [22–24] in which a secondary drop is generated only in the second step of coalescence cascade following the failure of the neck being pinched off in the first step of coalescence cascade.

Most previous studies have focused on the case where both the drop and interface are made of the same fluid, whereas only a few studies have been reported for the drop and interface made of different fluids. Because the transfer of surface energy to kinetic energy is so crucial in the coalescence, differences in surface tension between the drop and the interface caused by temperature or composition difference could be highly significant. Kavehpour [25] has published a detailed review work on the coalescence process, concluding that further research is needed to fully comprehend the influence of externally applied shear stresses such as viscous, electrical or Marangoni on the coalescence process during drop-interface or drop-drop coalescence. Blanchette *et al.* [26] explored the effect of mismatch surface tension between the drop and the liquid reservoir on the coalescence process using numerical and experimental work under zero and low Bond number conditions, respectively. They observed that partial coalescence is favored when the reservoir's surface tension, σ_2 , is higher than the droplet's surface tension, σ_1 , whereas total coalescence is favored when the reservoir's surface tension is lower. When $\sigma_2/\sigma_1 < 0.42$, the partial coalescence reappears and a new exciting phenomenon of an additional secondary drop ejection from the top of the merged

drop happens, mainly because of Marangoni stresses. Furthermore, they were unable to numerically replicate the drop ejection process which was later reproduced by Sun *et al.* [8] in their numerical study performed at zero Bond number. They also found the two different types of partial coalescence at low surface tension ratio: (i) peak ejection at low Ohnesorge number and (ii) bottom pinch-off at higher Ohnesorge number.

Blanchette [27] studied the mixing behavior of stationary as well as flowing droplets caused by either surface tension gradients or geometry effects, and concluded that the former is more important than the latter in terms of increasing mixing efficiency. The effect of varying surface tension caused by temperature difference have been explored by Saifi and Tripathi [28]. They reported that the coalescence behavior of cold drops differs significantly from that of hot ones, mainly at increasing temperature differences. They also showed that when a drop is kept colder than its surroundings, partial coalescence changes to total coalescence. However, the behavior of an isothermal system is unaltered, when the drop is kept hotter than its surroundings. The gradients of surface tension can also be generated by the use of surfactants and their effect on coalescence has been studied by several authors [29–31]. Recently, a new regime of coalescence cascade known as damped coalescence cascade has been discovered by Shim and Stone [32]. In this regime, the local Marangoni flow increased the drainage of the air between the secondary drop and the interface, resulting in the suppression of secondary drop rebound.

Along this path, we have seen that the coalescence process has been widely discussed for drop-reservoir and drop-drop interface in situations when both the drop and the interface are made of the same fluid. Drop-interfaces formed of dissimilar fluids have received little attention. Earlier studies [8,26] demonstrated the nonmonotonic behavior of partial coalescence caused by surface tension gradients for a drop coalescing on a flat liquid pool, but the same behavior has not been explored for the coalescence of two drops. Little importance has been given, in particular, to the partial coalescence of two drops with large surface tension difference. Furthermore, the effect of different parameters on coalescence of miscible drops, such as diameter ratio of two drops (also known as parent drop size ratio), viscosity and density ratio of both drops, and surface tension ratio [in both conditions: ($\sigma_1 > \sigma_2$) and ($\sigma_1 < \sigma_2$)] is still not thoroughly addressed; σ_1 and σ_2 being the surface tension of drop 1 and drop 2, respectively. Therefore, the goal of the present work is to numerically simulate the coalescence mechanism between two unequal-sized miscible drops for focusing the issues mentioned above. We investigated the quantitative and qualitative effects of the Ohnesorge number and surface tension ratio on contrast pinch-off regimes. The effect of parent drop size ratio on the coalescence of two drops with a large surface tension difference is also examined. A regime map is presented to provide a deeper understanding of the coalescence dynamics of two liquid drops that are miscible. The regime of second-stage pinch-off, which occurs between first-stage pinch-off and no pinch-off and was previously described solely for drop-interfaces composed of identical liquid, is shown for the coalescence of two miscible liquid drops.

The paper is organized as follows: in Sec. II, the numerical model and solution methodology are described in details. Section III presents the quantitative and qualitative comparison of the current simulation results with the experimental and theoretical results of previous studies from open literature. In Sec. IV, the influence of surface tension ratio, viscous forces, and parent drop size ratio on the coalescence behavior of two miscible liquid drops are presented and discussed. Finally, Sec. V summarizes the main points of results.

II. PHYSICAL DOMAIN AND SOLUTION METHODOLOGY

We have numerically examined the coalescence mechanism of two unequal-sized drops made of miscible but different fluids (as shown in Fig. 1). In a physical domain, the smaller drop of liquid-1 (i.e., upper drop) is positioned vertically just above the larger drop of liquid-2 (i.e., lower drop), with a small gap of $0.005D_u$ between them, where D_u is the upper drop diameter. It is worth mentioning that a small gap between two drops is required to prevent the formation of tangential stresses at the beginning of coalescence ($\tau = 0$). The lower drop and the surrounding air is initially

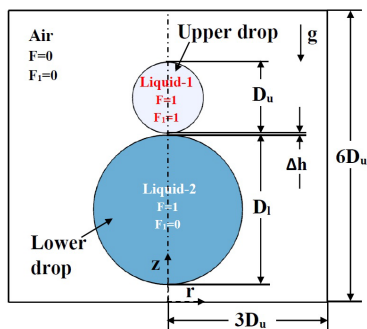


FIG. 1. Physical domain used for simulation showing coalescence of two unequal-sized miscible drops.

at rest, i.e., zero velocity, while the upper drop is set to a small nondimensional downward initial velocity of 0.001 just to trigger the coalescence process. The simulation is performed in a two-dimensional, axisymmetric cylindrical domain (r, z) using a coupled level set and volume of fluid method (CLSVOF). Here, r and z represent the radial and vertical directions, respectively, with $r = 0$ being the axis of symmetry. The computational domain has a width and height of $3D_u \times 6D_u$.

To highlight the effect of surface tension gradients on the cascade of partial coalescence, we have used water/ethanol or a water-ethanol mixture both for lower and upper drops. The main reason for choosing the above liquids is to minimize the effect of density and viscosity variations. The properties of both liquid-1 and liquid-2 are given elsewhere [26,33]. By varying the physical properties, the surface tension ratio, $\sigma_r = (\sigma_2/\sigma_1)$ is varied between 0.3 and 1.6. It is to be noted that the cases with $(\sigma_r < 0.3)$ can not be realized by using these two fluids as the minimum σ_r that can be obtained using water and ethanol drops is 0.3 only. Furthermore, when $\sigma_r < 1$, the upper drop and the lower drop are made of water and water-ethanol mixture, respectively, whereas the upper and lower drop is formed of ethanol and water-ethanol mixture, respectively, for $\sigma_r > 1$. The Ohnesorge number ($Oh = \mu_1/\sqrt{\rho_1\sigma_1 D_u}$) is varied in the range of 0.002 to 0.011, where ρ_1 and μ_1 are the density and viscosity, respectively, of the upper drop liquid. In the present study, the effect of gravity (g) is not considered and the coalescence is initiated where both drops are spherical. Therefore, the Bond number ($Bo = \rho_1 g D_u^2/\sigma_1$) is set to $Bo = 0$. This condition also ensures that the coalescence mechanism in the present work is mainly governed by the surface tension variations. Furthermore, it is important to note that although the effect of uneven surface forces and viscous forces on coalescence process are studied primarily for the condition where the parent drop size ratio ($D_r = D_l/D_u$) is 2.1 (i.e., the ratio of diameter of the lower drop is almost twice that of the upper drop), the parent drop size ratio (D_r) is also varied between 1 and 3 to analyze the effect of large surface tension difference between two drops (i.e., $\sigma_r = 0.3$). The detailed mathematical formulation used to perform simulation is described in the next section.

A. Governing equations

The system of coalescence process is characterized by mainly seven dimensionless parameters: the Bond number, $Bo = \rho_1 g D_u^2/\sigma_1$; the Ohnesorge number, $Oh = \mu_1/\sqrt{\rho_1\sigma_1 D_u}$; the Schmidt number, $Sc = \nu_1/k$; the surface tension ratio of lower drop to upper drop liquid, $\sigma_r = (\sigma_2/\sigma_1)$; the parent drop size ratio of lower drop to upper drop, $D_r = D_l/D_u$; the density ratio of liquid to gas, $\rho^* = \rho_l/\rho_g$; and the viscosity ratio of liquid to gas, $\mu^* = \mu_l/\mu_g$, where subscript l denotes either 1 or 2. ν_1 denotes the kinematic viscosity of upper drop liquid and k is the compositional diffusivity. In the present work, the typical values of ρ^* and μ^* are the order of $O(10^3)$ and $O(10^2)$, respectively, for a liquid-gas systems. Hence, the inertia and viscous effects from the surrounding air are assumed to be negligible. The governing equations are nondimensionalized by the upper drop diameter, D_u , as a length scale and $\tau = \sqrt{\rho_1 D_u^3/\sigma_1}$, as a timescale. The density, viscosity, and surface tension are

scaled using density, ρ_1 , viscosity, μ_1 , and surface tension, σ_1 , of the upper drop liquid. Pressure is scaled using capillary pressure as σ_1/D_u . Assuming all fluids are incompressible and Newtonian, the nondimensional continuity and momentum equation for our system are given as

$$\nabla \cdot \mathbf{V} = 0 \quad (1)$$

and

$$\rho^* \left[\frac{\partial \mathbf{V}}{\partial \tau} + \nabla \cdot (\mathbf{V}\mathbf{V}) \right] = -\nabla p + \text{Oh} \{ \nabla \cdot \mu^* [\nabla \mathbf{V} + (\nabla \mathbf{V})^T] \} + \rho^* \text{Bo} + F_\sigma, \quad (2)$$

where \mathbf{V} is the velocity field vector with radial (u) and vertical (v) components in the r and z directions, and p is the pressure. It is to be noted that the Bond number is set to zero in the present simulation. The forcing term F_σ is a surface δ function which is nonzero only on the interface and defined as [34]

$$F_\sigma = \delta(s) \nabla \cdot [(I - \hat{n}^T \hat{n}) \sigma^*] = \delta(s) (\nabla_s \sigma^* + \kappa \hat{n} \sigma^*) \quad (3)$$

Here κ is mean curvature of the interface, \hat{n} is unit normal vector, $\delta(s)$ is the Dirac δ function and ∇_s is a surface gradient operator defined on the interface. The tangential component of surface tension gradients is represented by the first term on the right-hand side of Eq. (3), whereas the normal component of surface tension force is represented by the second term. The first term is called Marangoni stresses. The use of potential forms for interfacial forcing terms reduces the numerical difficulties of dealing with interfacial forces.

A volume fraction function, F is used to distinguished the different fluid regions (liquid and gas) in a computational domain (see Fig. 1). The value of F is defined as 1 for liquid cells, 0 for gas cells and $0 < F < 1$ at the interface cell of gas and liquid. To achieve a smooth interface, a level set function ϕ has been used in terms of the signed distance function [35].

The movement of interface is tracked using the advection equations of F and ϕ as

$$\frac{\partial F}{\partial \tau} + \nabla \cdot (F\mathbf{V}) = F(\nabla \cdot \mathbf{V}), \quad (4)$$

$$\frac{\partial \phi}{\partial \tau} + \nabla \cdot (\phi\mathbf{V}) = \phi(\nabla \cdot \mathbf{V}). \quad (5)$$

One more tracking function, F_1 , is introduced into the flow for tracking the interface motion of between the lower and upper drop. The value of F_1 is 1 for upper drop liquid and 0 for lower drop liquid as shown in Fig. 1. For surrounding gas, the value of F_1 is 0. The interface between lower and upper drop is tracked using an advection-diffusion equation of F_1 as given by Blanchette *et al.* [26]:

$$\frac{\partial F_1}{\partial \tau} + \mathbf{V} \cdot (\nabla F_1) = \left(\frac{\text{Oh}}{\text{Sc}} \right) \nabla \cdot (k^* \nabla F_1), \quad (6)$$

where ($k^* = k/k_1$). We assume that the compositional diffusivity, k , is independent of F_1 to keep the number of computational parameters to a manageable level while only showing the effect of surface tension variations.

The Schmidt number, Sc , relates the importance of momentum transport to composition transport. For a liquid of density, viscosity and diffusion coefficient of the order of $\rho_l \sim O(10^3)$ kg/m³, $\mu_l \sim O(10^{-3})$ Pa s, and $k \sim O(10^{-9})$ m²/s, the value of Sc is set to a typical value of 1000 for water-ethanol liquid system [36].

The fluid properties (density, viscosity, and surface tension) are interpolated as

$$\rho^* = \frac{1}{\rho_1} \{ \rho_g(1 - F) + F[\rho_1 F_1 + \rho_2(1 - F_1)] \}, \quad (7)$$

$$\mu^* = \frac{1}{\mu_1} \{ \mu_g(1 - F) + F[\mu_1 F_1 + \mu_2(1 - F_1)] \}, \quad (8)$$

$$\sigma^* = \sigma_r F_1 + (1 - F_1). \quad (9)$$

B. Boundary conditions

The boundary conditions used to perform the numerical simulations are as follows:

At $r = 0$, a symmetry boundary condition has been imposed for velocity. This means that the normal component of velocity and tangential stress are set to be zero:

$$u = 0 \quad \text{and} \quad \frac{\partial v}{\partial r} = 0. \quad (10)$$

A no-slip impermeable wall boundary condition is applied on the bottom boundary:

$$u = 0 \quad \text{and} \quad v = 0. \quad (11)$$

The side walls are assumed to be placed sufficiently far from the drop interface so that they have no effect on dynamics of coalescence process. Therefore, the same boundary condition as the symmetry axis is defined for the right boundary surface.

The top confining surface is treated as an open boundary, hence zero Neumann condition has been imposed there:

$$\frac{\partial u}{\partial z} = 0 \quad \text{and} \quad \frac{\partial v}{\partial z} = 0. \quad (12)$$

Zero Neumann boundary condition has been imposed for pressure at all surfaces except at the top confining surface where pressure is defined as the atmospheric pressure (p_{atm}).

For volume fraction function (F and F_1) and level set function ϕ , zero Neumann boundary condition has been applied on all boundary surfaces.

C. Solution algorithm

A CLSVOF method-based in-house developed code is used to performed the numerical simulations. A fixed collocated grid is adopted to compute velocity, pressure, volume fraction, and level set function. The governing equations are discretized using a finite volume methodology. A second-order central difference scheme is used to approximate the convective terms and diffusive terms of Eqs. (2) and (6). The convective term of level set equation is discretized using second-order central difference scheme. Implicit method has been implemented for time advancement. With known values of volume fraction function (F^n and F_1^n), the fluid properties are calculated from Eqs. (7)–(9). A two-step predictor-corrector method is employed to obtain the velocity and pressure field at the new time step, τ^{n+1} . For reconstruction and advection of interface, the advection equations, Eqs. (4) and (5) are solved using a coupled second-order conservative operator splitting method [37–41]. The detailed documentation of algorithm can be found elsewhere [42,43]. A feasible time-step is calculated on the basis of the stability criterion [21,38] for all simulation cases and fixed as $\Delta\tau = 10^{-4}$.

D. Energy analysis

In the present study, we evaluated the energy budget for the coalescence of two miscible liquid drops. The total energy (TE) of the system should be constant throughout the coalescence process, and equal to the sum of the initial kinetic energy [$(E_{\text{ke}})_{\text{init}}$] and the initial surface energy [$(E_{\text{se}})_{\text{init}}$], according to the energy conservation law. In each time level, the total energy must also be equal the sum of the kinetic, surface, and total dissipation energy. The energy balance can be expressed mathematically as

$$TE = (E_{\text{ke}} + E_{\text{se}})_{\text{init}} = E_{\text{ke}}(\tau) + E_{\text{se}}(\tau) + E_{\text{de}}(\tau) \quad (13)$$

At each time step throughout the coalescence process, the nondimensional kinetic energy, surface energy, and total dissipation energy are calculated as follows:

$$E_{\text{ke}} = \frac{1}{2} \sum_{i,j=1}^{N_{\text{cells}}} \rho^* (u_{i,j}^2 + v_{i,j}^2) V_{\text{cell}}, \quad (14)$$

$$E_{se} = \sum \sigma^* A_s, \quad (15)$$

$$E_{de} = \int_0^\tau \left(\sum_{i,j=1}^{N_{\text{cells}}} (\text{VDR}) V_{\text{cell}} \right) d\tau, \quad (16)$$

where V_{cell} and N_{cells} represent the volume and number of computational cell, $u_{i,j}$ and $v_{i,j}$ define the velocity components in r and z direction and A_s denotes the surface area.

The nondimensional local viscous dissipation rate, VDR is computed as follows:

$$\text{VDR} = \mu^* (\text{Oh}) \left[2 \left(\frac{\partial u}{\partial r} \right)^2 + 2 \left(\frac{\partial v}{\partial z} \right)^2 + 2 \left(\frac{u^2}{r^2} \right) + \left(\frac{\partial u}{\partial z} + \frac{\partial v}{\partial r} \right)^2 \right]. \quad (17)$$

III. CODE VALIDATION

The in-house code used in the present work is significantly validated earlier [42,43] for numerous problems related to drop impact on thin films and coalescence of two identical liquid drops. However, in the present work, we have further validated our code by successfully reproducing the experimental results of Blanchette and Bigioni [10] and Anilkumar *et al.* [2]. For quantitative comparison, the experimental results of Thoroddsen *et al.* [44], and the theoretical model of Koldewej *et al.* [45] have been adopted. It should be noted that a 3D representation of the present axisymmetric simulation results is shown in Fig. 2 for better visualization and understanding of the physics of the problem.

A. Qualitative study

Figure 2(a) shows the temporal evolution of partial coalescence of an ethanol drop impacting on an ethanol liquid pool. The dimensionless parameters used in the simulation are as follows: $\text{Oh} = 0.008$, $\text{Bo} = 0.4$, and $\sigma_r = 1.0$. It is found that the interface evolution from drop deformation, neck development to secondary drop pinch-off are in good agreement with the experimental results of Blanchette and Bigioni [10]. The coalescence sequence of two highly viscous silicon oil drops in the presence of water is depicted in Fig. 2(b). The simulation parameter used for this condition are as follows: $D_r = 1.75$, $\text{Oh} = 0.203$, $\rho_1/\rho_g = 0.96$, $\mu_1/\mu_g = 99$, and $\sigma_r = 1.0$. The present results indicate a very good agreement with experimental results of Anilkumar *et al.* [2] as the two drop do not show any merging. The smaller drop simply lodged on the large drop forming a dome shape due to high viscous effect.

B. Quantitative study

In Fig. 3(a), the temporal evolution of local neck radius, R_{neck} for the coalescence of two water drops is compared with the experimental results of Thoroddsen *et al.* [44] both qualitatively and quantitatively. The condition of the simulation are: $D_r = 1.07$, $\text{Oh} = 0.0035$, $\text{Bo} = 0.15$, $\sigma_r = 1.0$. The hollow circles belong to Thoroddsen *et al.* [44] experimental data and solid line represent the actual numerical simulation data. The solid circle describes the evolution of neck shape at six different time steps. Our numerical results match very well with experimentally observed values of local neck radius, R_{neck} . Also, the interface dynamics obtained in the present simulation (shown by cyan color) are in good agreement with experimental results of Thoroddsen *et al.* [44].

To further validate the code in correctly capturing the Marangoni flow, another quantitative comparison has been done with the theoretical model of Koldewej *et al.* [45] given for spreading length of lower surface tension fluid in the higher surface tension fluid during drop coalescence as shown in Fig. 3(b). The condition of the simulation are: $D_r = 2.1$, $\sigma_r = 1.53$, and two different Ohnesorge numbers, i.e., $\text{Oh} = 0.0035$ and 0.007 . We extracted the spreading length $[L(t)]$ [see Fig. 3(b)] at different time steps and followed Koldewej *et al.* [45] to normalize the $L(t)$ and time, t . $L(t)$ is normalized by $L(t)^* \sim L(t)/[\mu_1^2/(\rho_1 \Delta\sigma)]$ and t is normalized by $t^* \sim t/[\mu_1^3/(\rho_1 \Delta\sigma^2)]$. It

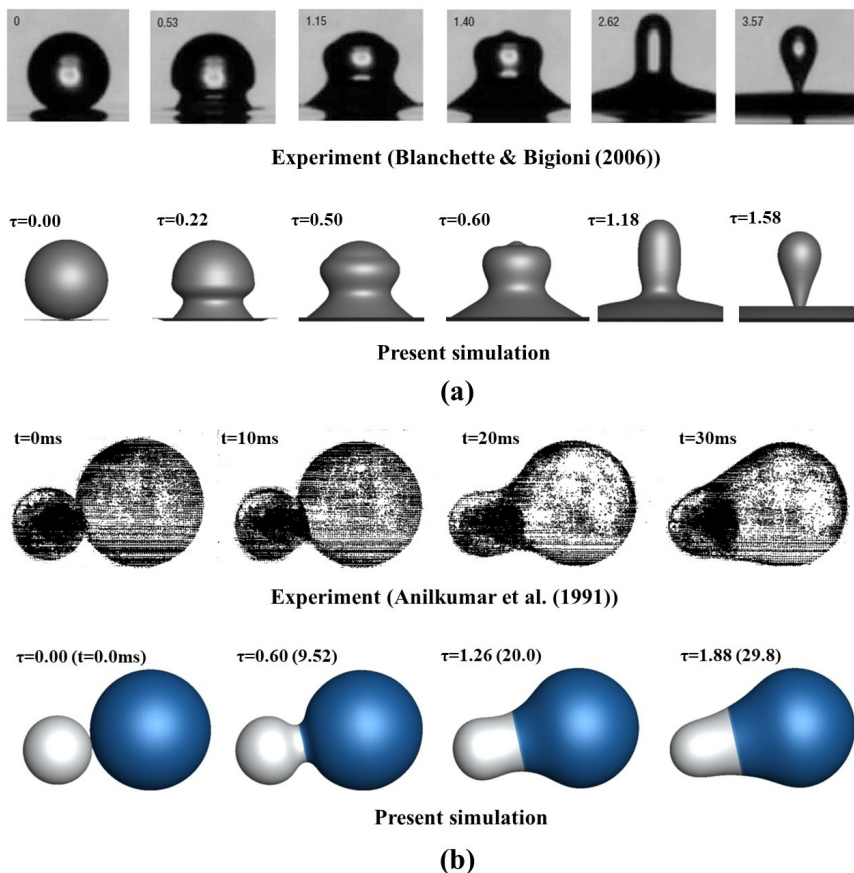


FIG. 2. Qualitative validation of present numerical results (bottom row) with experimental results of (a) Blanchette and Bigioni [10] (top row) for partial coalescence of an ethanol drop with an ethanol liquid pool for $Oh = 0.008$, $Bo = 0.4$ and $\sigma_r = 1.0$, and (b) Anilkumar *et al.* [2] (top row) showing the coalescence of two different-sized drops of diameter ratio, $D_r = 1.75$. The other relevant parameters are $Oh = 0.203$, $\rho_l/\rho_g = 0.96$, $\mu_l/\mu_g = 99$, and $\sigma_r = 1.0$.

can be observed that our simulation successfully reproduces the theoretical scaling law of Koldewej *et al.* [45] [$L(t)^* \sim t^{*3/4}$].

C. Grid independence study

The grid independence test has been done for three different grid sizes: 362×724 , 542×1084 and 814×1628 for the coalescence of two unequal drop sizes. The simulation is performed under following conditions: $D_r = 2.1$, $\sigma_r = 1.53$, and $Oh = 0.0035$. Comparison of interface shape profile at $\tau = 0.32$ and formation of third secondary drop at $\tau = 1.24$ are presented in Fig 4. Table I compares the size of the first, second, and third secondary drop, i.e., $(r_d)_1$, $(r_d)_2$, and $(r_d)_3$, respectively, generated during coalescence of two drops resulting in first-stage pinch-off at different grid sizes. It is found that the first and second secondary drop formation is captured by all three grid sizes, however, only the intermediate, 542×1084 , and the finest grid, 814×1628 , are capable of capturing the third secondary drop generation as depicted in Fig. 4(b) and Table I. Also, the difference in interface profiles is found to be almost negligible between the intermediate and the finest grid sizes (see Fig. 4). The drop tip formation and third secondary drop pinch-off are captured very well in the case of the intermediate and finest grids. Table I shows that the difference

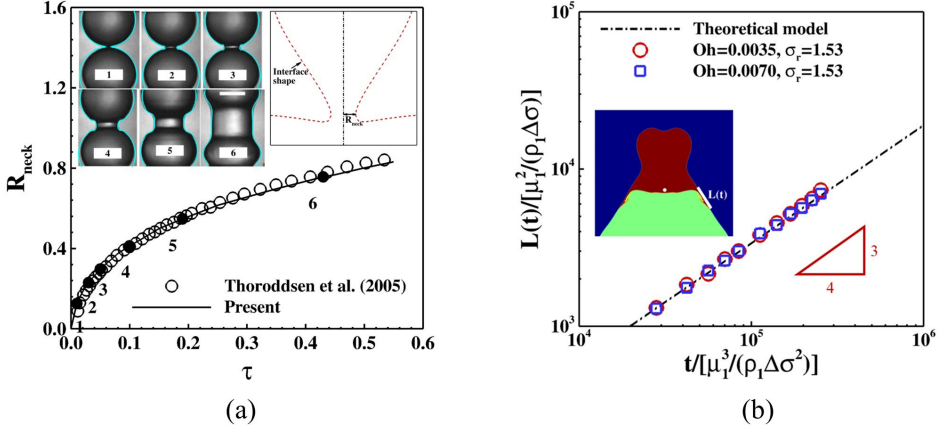


FIG. 3. Quantitative validation of present numerical results with (a) experimental results of Thoroddsen *et al.* [44] for temporal evolution of local neck radius, R_{neck} under following simulation parameters: $D_r = 1.07$, $\text{Oh} = 0.0035$, $\text{Bo} = 0.15$, $\sigma_r = 1.0$, and (b) theoretical model of Koldewej *et al.* [45] for spreading length of the lower surface tension liquid into the higher surface tension liquid for $D_r = 2.1$ and $\sigma_r = 1.53$.

in $(r_d)_1$ values is almost negligible for three different grid sizes. The percentage difference in $(r_d)_2$ value between coarser grid, 362×724 , and intermediate grid, 542×1084 , is around 7.3%, while the difference reduces significantly to 0.9% between the intermediate and the finest grid, 814×1628 . The percentage difference in $(r_d)_3$ values between the intermediate grid, 542×1084 , and the finest grid, 814×1628 , is 1.07. In our simulation, we have taken the grid size of 542×1084 as this grid size provides the grid independent results.

D. Domain independence study

The computational domain ($3D_u \times 6D_u$) has taken to be sufficiently large so that the side confining surfaces are positioned sufficiently far from the drop interfaces and the boundary conditions have no effect on the dynamics of coalescence process. The domain independence test has been performed using two different domain sizes: $3D_u \times 6D_u$ and $4.5D_u \times 9D_u$. The integral parameters obtained

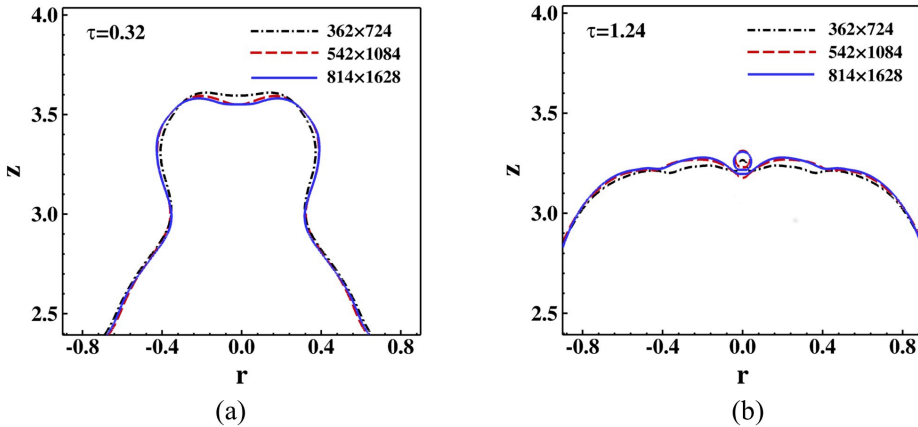


FIG. 4. Comparison of (a) drop tip deformation, and (b) third secondary drop generation for different grid sizes plotted at time step, $\tau = 0.32$ and $\tau = 1.24$, respectively. The other parameters are $D_r = 2.1$, $\sigma_r = 1.53$, and $\text{Oh} = 0.0035$.

TABLE I. Secondary drop size ratio in case of first-stage pinch-off for different grid resolution having $D_r = 2.1$. The values of other parameters are $\sigma_r = 1.53$ and $\text{Oh} = 0.0035$. Here D_1 , D_2 , and D_3 are the diameter of the first, second, and third secondary drops, respectively.

Grid size	$(r_D)_1 = D_1/D_u$	$(r_D)_2 = D_2/D_u$	$(r_D)_3 = D_3/D_u$
362×724	0.5701	0.2532	No secondary drop
542×1084	0.5712	0.2731	0.1014
814×1628	0.5718	0.2756	0.1025

using the two domain sizes have been listed in Table II. The discrepancies in the $(r_d)_1$, $(r_d)_2$, and $(r_d)_3$ values for the partial coalescence are found to be 0.05%, 0.7%, and 1.4% between two sets of results, respectively. Therefore, all simulations are done using the domain size of $3D_u \times 6D_u$.

IV. RESULTS AND DISCUSSION

We investigated the effects of surface tension gradients, Ohnesorge number, and parent drop size ratio on the coalescence dynamics of two unequal-sized drops. A regime map on the $\text{Oh}-\sigma_r$ plane is also drawn to depict the various coalescence regimes. The influences of the surface tension ratio, Ohnesorge number, and parent drop size ratio on the estimated kinetic, surface, and dissipation energies during the coalescence process are discussed.

A. Effect of surface tension ratio

In Fig. 5, the secondary drop generation of liquids with uniform surface tension is compared to liquids with uneven surface tensions. The Oh and D_r is fixed at $\text{Oh} = 0.0035$ and $D_r = 2.1$ for all the cases, while the σ_r is increased by increasing the surface tension of lower drop liquid. A 3D view of 2D axisymmetric results are shown in Fig. 5 for a better visualization of coalescence of two miscible drops. It is found that the coalescence process produces a nonmonotonic results from partial coalescence [Figs. 5(d), 5(e) and 5(f)] to no pinch-off [Figs. 5(b) and 5(c)] and again back to partial coalescence [Fig. 5(a)] with a reduction in σ_r . The partial coalescence shown in Figs. 5(a), 5(e) and 5(f) are categorized as first-stage pinch-off because the drop deformation, neck development, and secondary drop creation occur in the same manner as a drop coalescing into a flat liquid pool. There is also a transition region between the first-stage pinch-off and no pinch-off, where the second-stage pinch-off occurs [Fig. 5(d)].

The partial coalescence process is observed to be completed in two stages: in the first, the two drops are connected by a neck that expands radially outwards causing a capillary surface wave to propagate upward towards the drop apex, while in the second, the neck narrows radially inward with an interface retracting downward. Finally, the pinch-off occurs around the initial point of contact. When considering only the radial motion of the neck, which is driven by the net capillary pressure $[\sigma(\kappa_\theta - \kappa_x)]$, the azimuthal curvature ($\kappa_\theta = 1/R_{\text{neck}}$) is found to be much smaller than the axial curvature ($\kappa_x = 1/R_{\text{axn}}$) in the first stage (i.e., $\kappa_\theta \ll \kappa_x$) when the neck expands, but it increases significantly in the second stage (i.e., $\kappa_\theta \gg \kappa_x$), when the neck shrinks. Here κ_θ and κ_x are the

TABLE II. Secondary drop size ratio generated during the coalescence of two miscible drops, resulting in a first-stage pinch-off with $D_r = 2.1$ for two different domain sizes. The values of other parameters are $\sigma_r = 1.53$ and $\text{Oh} = 0.0035$. Here D_1 , D_2 , and D_3 are the diameter of the first, second, and third secondary drops, respectively.

Grid size	$(r_d)_1 = D_1/D_u$	$(r_d)_2 = D_2/D_u$	$(r_d)_3 = D_3/D_u$
$3D_u \times 6D_u$	0.5712	0.2731	0.1014
$4.5D_u \times 9D_u$	0.5709	0.2750	0.1000

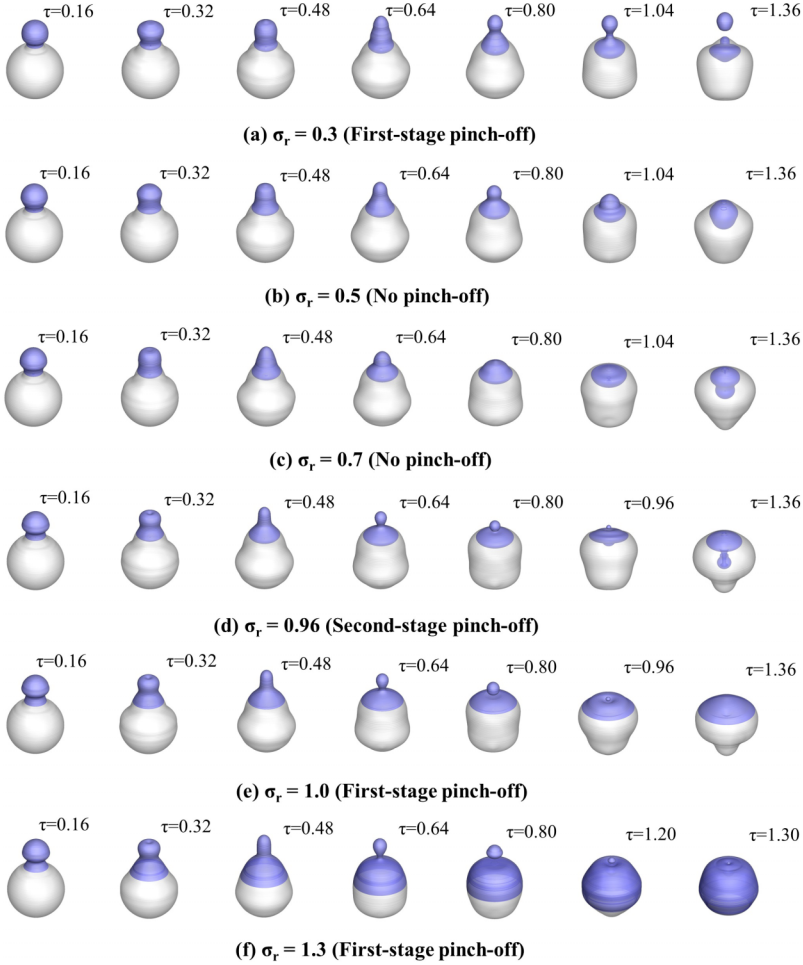


FIG. 5. Different pinch-off regimes obtained during the coalescence of two unequal-sized drops for $Oh = 0.0035$ and $D_r = 2.1$ at varying surface tension ratio (σ_r).

azimuthal and axial curvature of the neck [see Fig. 14(b) for definition of axial and azimuthal curvature]. Due to the decreased axial curvature in the second stage, the fluid is squeezed away from the neck by the strong radially inward capillary forces, resulting in a secondary drop pinch-off [22]. Therefore, to achieve partial coalescence, the horizontal rate of collapse must be high enough that vertical collapse is delayed and the neck has a shaper azimuthal curvature during its final contraction.

As shown in Fig. 5(e), the first-stage pinch-off for $\sigma_r = 1.0$ occurs in a manner similar to that described in many prior studies [10,46] such as coalescence of a drop in a liquid reservoir. The outcome is again a first-stage pinch-off for $\sigma_r = 1.3$ [Fig. 5(f)], and the coalescence steps are qualitatively similar to the $\sigma_r = 1.0$ case. However, in the case of $\sigma_r = 1.3$, the resulting secondary drop appeared to be slightly bigger than in the case of $\sigma_r = 1.0$. Overall, the entire coalescence cascade of $\sigma_r = 1.3$ shows very little deviation from the $\sigma_r = 1$ scenario. For $\sigma_r < 1$ situations, the coalescence process exhibits more complex behaviors. When the σ_r is decreased, i.e., $\sigma_r = 0.5$ and 0.7 [Figs. 5(b) and 5(c)], the outcome is no pinch-off and the droplet merges fully into the bulk liquid.

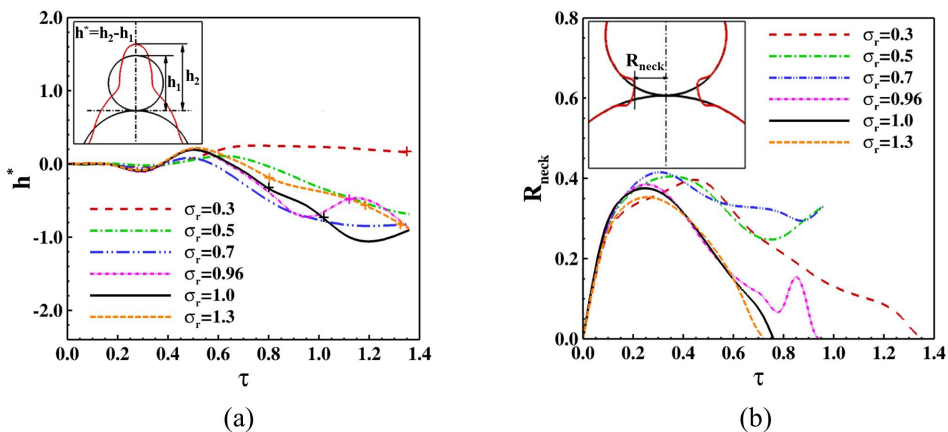


FIG. 6. Effect of surface tension ratio (σ_r) on temporal evolution of (a) h^* and (b) R_{neck} . The other nondimensional parameters are $D_r = 2.1$ and $\text{Oh} = 0.0035$.

Whenever σ_r is not equal to 1.0, the higher surface tension liquid pushes on the droplet interface, generating a tangential flow that partially covers the higher surface tension liquid's surface with the lower surface tension liquid. Therefore, when $\sigma_r < 1$, the lower droplet's liquid (which has lower surface tension) climbs up the sides of the upper droplet (which has higher surface tension), resulting in a reduction of local surface tension at the droplet interface, which drives the radial constriction. As a result, the vertical rate of collapse becomes dominant and begins to push the liquid downward, resulting in no pinch-off [as observed in Figs. 5(b) and 5(c)]. Sun *et al.* [8] mentioned that the timescale of capillary forces that governs the horizontal rate of collapse can be estimated using $\sqrt{\rho_1 D_u^3 / \sigma_1}$. Because $\sqrt{\rho_1 D_u^3 / \sigma_1} / \sqrt{\rho_1 D_u^3 / \sigma_2} = \sqrt{1 / \sigma_r} > 1$, so lowering the local surface tension at the drop interface surface from σ_1 to σ_2 would eventually result in a delayed horizontal collapse.

The first-stage pinch-off re-emerges as σ_r is reduced further, as shown in Fig. 5(a) for $\sigma_r = 0.3$. In comparison to the $\sigma_r = 1.0$ scenario, where pinch-off happens at $\tau = 0.74$, it is found that in this case, the neck pinches off at a considerably longer time instant, $\tau = 1.34$. If we compare the ratio of pinch-off times of above-mentioned cases, then we get 1.81 which closely equal to the value of $\sqrt{1 / \sigma_r}$. This suggests that the pinch-off is caused solely by the horizontal rate of collapse, with a partial coalescence reappearing as a result of the prolonged vertical collapse. It is also observed that the initial coalescence stages from neck opening to capillary wave propagation to upward stretching of drop are found to be similar to those seen in the $\sigma_r = 1.0$ case. However, the upward stretching in the $\sigma_r = 0.3$ case is significantly more pronounced than the $\sigma_r = 1.0$ case mainly due to the presence of the tangential Marangoni stresses.

It is also worth mentioning that no secondary droplet forms when σ_r is less than or equal to 0.95. When $\sigma_r > 0.985$, the first-stage pinch-off happens. A transition region exists between the first-stage pinch-off and no pinch-off, where the pinching neck re-expands without causing a secondary drop in the first step and the pinch-off occurs in the second step of the coalescence cascade [Fig. 5(d) for $\sigma_r = 0.96$]. The pinch-off is referred to as a second-stage pinch-off. This form of coalescence cascade has been previously reported for droplets made of the same liquid [22,24]. However, the second-stage pinch-off is also found to occur for droplets made of miscible liquids as shown in Fig. 5(d). Between pinch-off and no pinch-off regime, the second-stage pinch-off is observed for a very narrow range of $\sigma_r = 0.95$ to 0.985 (see Fig. 23, at $\text{Oh} = 0.0035$ for the above mentioned values of σ_r).

The temporal evolution of the relative height of the upper drop apex (h^*) and the neck radius (R_{neck}) for various σ_r are compared in Figs. 6(a) and 6(b) to analyze the impact of Marangoni flow on the vertical and horizontal rate of collapse that leads to the nonmonotonic emergence of partial

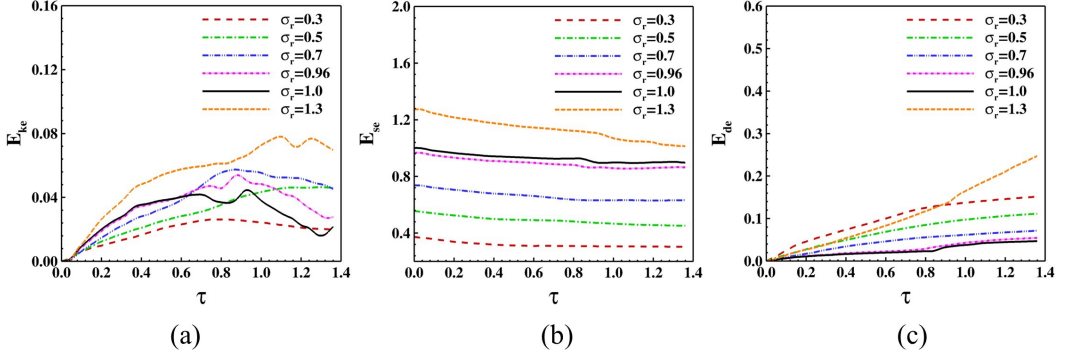


FIG. 7. Effect of surface tension ratio (σ_r) on temporal evolution of (a) the kinetic energy (E_{ke}), (b) the surface energy (E_{se}), and (c) the dissipation energy (E_{de}) for $Oh = 0.0035$ and $D_r = 2.1$.

coalescence. The simulation parameters are identical to those described in Fig. 5. As shown in Fig. 6(a), the flow caused by the neck expansion has no effect on the h^* during the initial stage of coalescence ($\tau < 0.35$). The maximum vertical stretching of the upper drop apex is observed for the $\sigma_r = 0.3$ case due to increased upward movement generated by large Marangoni forces. When the σ_r is increased to 0.5 or 0.7, the upward stretching motion of the droplet is suppressed even before it merges more quickly with the bulk liquid. The reason for this is that the lower surface tension liquid partially covers the drop interface, reducing interfacial oscillation. The droplet apex is lifted again by the upward propagating capillary waves when the σ_r is increased further up to 1.3 (i.e., $\sigma_r = 0.96, 1, \text{ and } 1.3$). It is also visible from figure that the value of maximum h^* is slightly higher for $\sigma_r = 1.3$ case than for $\sigma_r = 1$ case.

The temporal trajectories of neck radius (R_{neck}) for different σ_r in Fig. 6(b) reveals that as σ_r decreases from 1.3 to 0.3, the total time for the upper drop completely merging into the lower drop increases. The transition to no pinch-off takes place corresponding to $\sigma_r = 0.96$ with the upper drop oscillating two times before being absorbed by the lower drop. The number of neck radius oscillations reduces to one, when the value of σ_r is further increased ($\sigma_r = 1.0$) or decreased ($\sigma_r = 0.7$). The dual (twice) oscillation in neck radius for $\sigma_r = 0.96$ indicates that the pinch-off occurs in the second step of the coalescence cascade, resulting in the second-stage pinch-off process. At a smaller σ_r values (i.e., between $\sigma_r = 0.3$ and $\sigma_r = 0.5$), however, the second stage pinch-off becomes absent. The maximum spreading of the neck is obtained for no pinch-off cases ($\sigma_r = 0.5$ and 0.7) which can be attributed to strong Marangoni forces. In comparison to $\sigma_r = 1.0$, the maximum value of R_{neck} decreases and the pinch-off occurs earlier for $\sigma_r = 1.3$ case.

The temporal evolution of the kinetic energy, surface energy and dissipation energy are shown in Figs. 7(a), 7(b) and 7(c), respectively. The energies are calculated using Eqs. (14)–(16), and are normalized by the initial surface energy of drops with $D_r = 2.1$ and $\sigma_r = 1.0$. The initial surface energy is chosen for normalization because, in stationary drops coalescence, the total energy of the system at $\tau = 0$ is primarily composed of the surface energy of two drops. Furthermore, using the initial surface energy of $\sigma_r = 1.0$, a clear picture of the effect of different parameters on the coalescence process has been presented. The temporal evolution of the kinetic energy plots reveals that $\sigma_r = 1.3$ has the highest kinetic energy and $\sigma_r = 0.3$ has the lowest [see Fig. 7(a)]. This happens because the initial surface energy is higher when the σ_r is larger. The surface energy at $\tau = 0$ for two drops is written as

$$(E_{se}) = \pi D_u^2 \sigma_1 + \pi D_l^2 \sigma_2 = \pi D_u^2 \sigma_1 (1 + \sigma_r D_r^2). \quad (18)$$

It is simple to conclude from Eq. (18) that for a fixed D_r , when σ_r decreases, most part of the initial surface energy reduces. As the coalescence process advances, the initial surface energy is converted into kinetic energy, and the remaining surface energy is dissipated by viscosity [see Figs. 7(b)

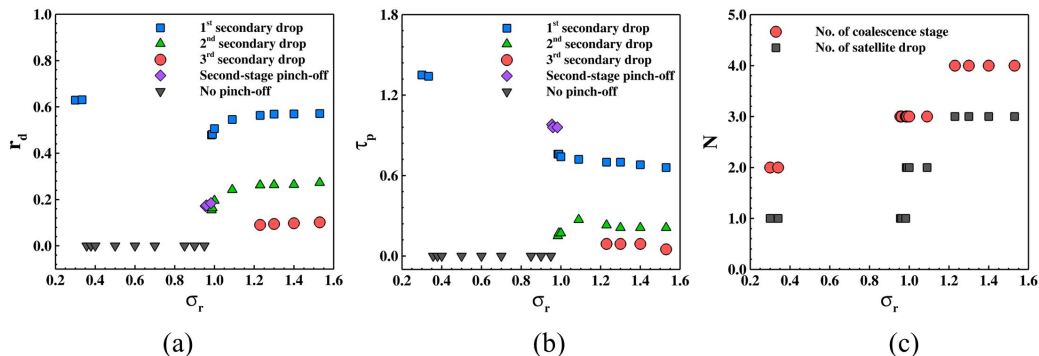


FIG. 8. Effect of surface tension ratio (σ_r) on (a) variation of r_d , (b) τ_p (measured from the start of coalescence upto the secondary drop generation), and (c) total number of coalescence stage and secondary drops produced. The other dimensionless parameters are $D_r = 2.1$ and $Oh = 0.0035$.

and 7(c)]. The presence of Marangoni forces causes the kinetic energy to decrease with decreasing σ_r . The kinetic energy for $\sigma_r = 0.96$ and 1 falls rapidly as the neck pinches off to produce a secondary drop. For $\sigma_r = 0.96$, the kinetic energy reduces slightly at first, then rises as the neck fails to pinch-off in the first step, and finally decreases rapidly as the neck breaks up in the second step of the coalescence cascade. The number of oscillations in the kinetic energy curve (i.e., 2 and 3, respectively) for $\sigma_r = 1.0$ and 1.3 equals the number of secondary drops produced as seen in Fig. 5. In addition, the decrease in surface energy at later time instants is higher for $\sigma_r = 1.3$ than for other σ_r cases, resulting in an increase in dissipation energy at later time instants for $\sigma_r = 1.3$ [see Figs. 7(b) and 7(c)].

The influence of varying σ_r on the secondary drops generated during first-stage pinch-off (i.e., first, second, and third secondary drops), second-stage pinch-off, $\sigma_r = 0.3$ and pinch-off time are summarized in Fig. 8. The simulation is performed under the same conditions as mentioned in Fig. 5. As demonstrated in Figs. 8(a) and 8(b), a lower σ_r (i.e., $\sigma_r < 0.35$) yields larger secondary droplets, although secondary drop formation also occurs at a longer pinch-off time (pinch-off time is measured from the initiation of coalescence to the secondary drop generation). This happens because Marangoni flow persists on the interface for a prolonged period of time after the initial convergence at the droplet apex, delaying the secondary drop pinch-off. It also means that the advancing front of the lower surface tension liquid from the lower droplet slows down as it wraps up the upper droplet, resulting in an enhanced mixing owing to Marangoni flow.

The pinch-off phenomenon does not occur for $0.35 < \sigma_r \leq 0.95$. It is also visible from Figs. 8(a) and 8(b) that the secondary drop size and the pinch-off time for both first and second secondary drops are greatly affected with the variations in σ_r when $\sigma_r < 1.1$. However, as σ_r is increased (i.e., $\sigma_r > 1.1$), the r_d and τ_p for all secondary drops (first, second, and third) slightly rise and decrease, respectively. This is mostly due to an increase in the kinetic energy of the drop [see Fig. 7(a)], which causes a reduction in the expansion of the neck, hence increasing the volume of the secondary drops. Moreover, at a larger value of σ_r , the total time between shrinking of the neck and the secondary drop formation reduces. This helps to explain why the pinch-off time is shorter for larger σ_r [Fig. 8(b)]. Furthermore, the secondary drop generation in the second-stage pinch-off is also observed to occur at a longer pinch-off time.

It is also noticed that the size of secondary drops attained for $\sigma_r < 0.35$, $\sigma_r > 1.0$ and second-stage pinch-off are almost 1.2, 1.12, and 0.3 times that of the first secondary drop obtained at $\sigma_r = 1$, respectively. When $\sigma_r = 0.955$, i.e., during second-stage pinch-off, the smallest secondary drop having a size of 0.17 is generated. The size of largest secondary drop obtained for $\sigma_r = 0.33$ is $r_d = 0.63$. As illustrated in Fig. 8(c), both the number of coalescence stages and the number of

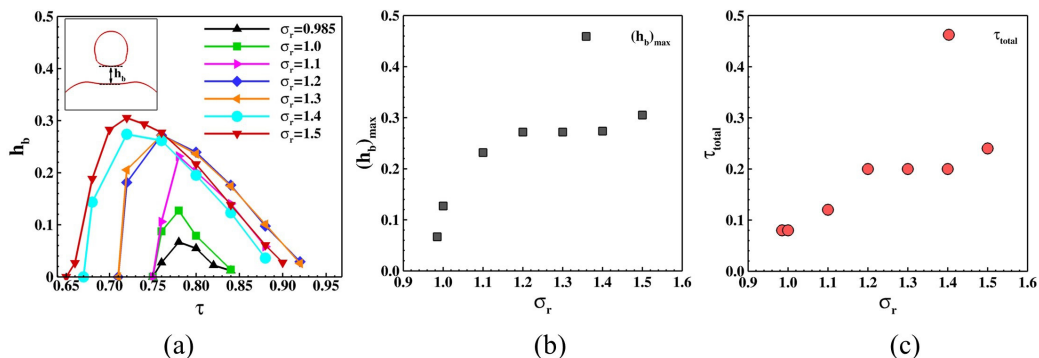


FIG. 9. (a) Effect of surface tension ratio (σ_r) on the temporal evolution of the first secondary drop jumping height, h_b , (b) $(h_b)_{\max}$ versus σ_r , and (c) τ_{total} taken by the first secondary drop from pinch-off to again come into contact with the interface versus σ_r . The values of other nondimensional parameters are $D_r = 2.1$ and $Oh = 0.0035$.

secondary drops increases as the σ_r increases. The averaged size of the first, second, and third secondary drops are found to be 0.57, 0.47, and 0.36, respectively, for $\sigma_r > 1.1$.

The role of increasing kinetic energy as the σ_r varies can also be seen from Fig. 9, where the temporal evolution of the dynamics of the first secondary drop is plotted. The other nondimensional parameters are the same as mentioned in Fig. 5. As shown in Fig. 9(a), the jumping height, h_b increases as the secondary drop moves upwards after pinching off, achieves its maximum, and then decreases as the secondary drop comes downwards in all cases. Up to $\sigma_r = 1.1$, the starting position of h_b curve is same for $\sigma_r = 0.985, 1.0$ and 1.1 as the pinch-off time for the first secondary drop is found to be the same for all three cases. However, once σ_r is increased from 1.1, the curve began to shift to the left as the secondary drop detaches earlier, resulting in a decrease in pinch-off time, as illustrated in Fig. 9(a). The secondary drop at the highest σ_r ($\sigma_r = 1.5$) takes longer to reach the $(h_b)_{\max}$ due to the increased volume of the drop at the highest σ_r . Furthermore, the total time duration (τ_{total}) taken by the first secondary drop from pinch-off to its return to the interface increasing with σ_r before becoming asymptotic at higher σ_r [see Fig. 9(c)]. Similarly, the maximum bouncing height, $(h_b)_{\max}$ is found to show identical variation [see Fig. 9(b)] as that of τ_{total} which believed to be due to increased kinetic energy as seen in Fig. 7(a).

Aside from that, one can see from Figs. 5 and 10 how the coalescence cascade of drops having distinctly liquids differs from the coalescence cascade of drops made of the same liquids. When $\sigma_r > 1.0$, the surface tension mismatch affects just the first coalescence event. Subsequent coalescence events, however, would almost certainly occur between a drop and an interface surface with the same local composition as the first generated secondary drop. Because the surface tension gradient has only a little effect on the first secondary drop, previous partial coalescence descriptions [9] apply to $\sigma_r > 1.0$ as well [see Fig. 10(a)]. The gradient in surface tension for $\sigma_r < 1.0$ cases is observed to span across a significantly greater length scale with the lower drop liquid spreading over the upper droplet surface [as shown by the mix color region in Fig. 10(b)], rather than being confined to the area of the contact point where the two dissimilar fluids initially join. Also, the secondary drops in this case appear to be a combination of both lower and upper drop liquids.

High vorticity generation from the advancing Marangoni flow causes enhanced mixing inside the upper drop for cases with $\sigma_r < 1.0$ [see the vorticity field in Fig. 11(a)]. For $\sigma_r > 1.0$ cases, however, vorticity formation is more confined to the vicinity of the lower drop surface, with the strongest vorticity generation occurring around the neck region in the form of a vortex, as shown in Fig. 11(b). In addition, this vortex no longer exists for the cases depicted in Fig. 11(a). The gradients in surface tension also favor the detachment of the vortex ring generated during coalescence from the upper drop liquid from the interface surface, as shown in Fig. 10(b) at $\tau = 1.36$; hence, any

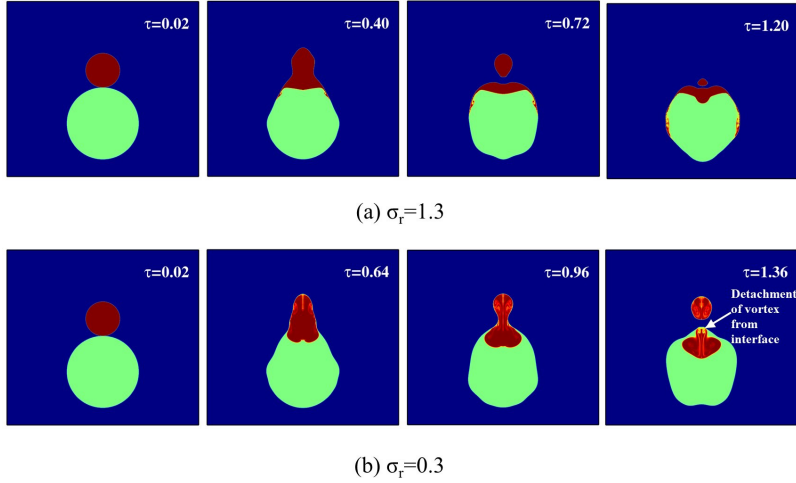


FIG. 10. Evolution of interface shape and mixing pattern generated by surface tension mismatch for (a) $\sigma_r = 1.3$ and (b) $\sigma_r = 0.3$. The upper drop, lower drop, and the surrounding air is shown by red, green, and blue color, respectively. The other nondimensional parameters are $D_r = 2.1$ and $Oh = 0.0035$.

secondary drop would approach an interface with a composition similar to that of the initial interface [see Fig. 10(b)].

Previous studies [10,20,21] have revealed that the horizontal rate of collapse controls the pinch-off process, whereas the vertical collapse favors no pinch-off. To demonstrate this, we plotted in Fig. 12 snapshots of the radial velocity, vertical velocity and pressure fields for different values of σ_r at two distinct time steps: $\tau = 0.32$ and $\tau = 0.64$ for $\sigma_r = 0.7, 1.0$ and 1.3 ; and $\tau = 0.44$ and 0.96 for $\sigma_r = 0.3$. The other dimensionless parameters are identical as shown in Fig. 5. Cases $\sigma_r = 0.3, 1.0,$ and 1.3 result in first-stage pinch-off, whereas case $\sigma_r = 0.7$ results in no pinch-off (also shown in Fig. 5). Although the graphs are shown at the same time-step ($\tau = 0.32$) for $\sigma_r = 0.7, 1.0,$ and 1.3 , the development of the coalescence process is more advanced with increasing σ_r with more deformed drop tip obtained for larger σ_r (i.e., $\sigma_r = 1.3$). The height of liquid column for $\sigma_r = 1.3$ is also found to increase significantly as compared to $\sigma_r = 1.0$ at $\tau = 0.64$. However, due

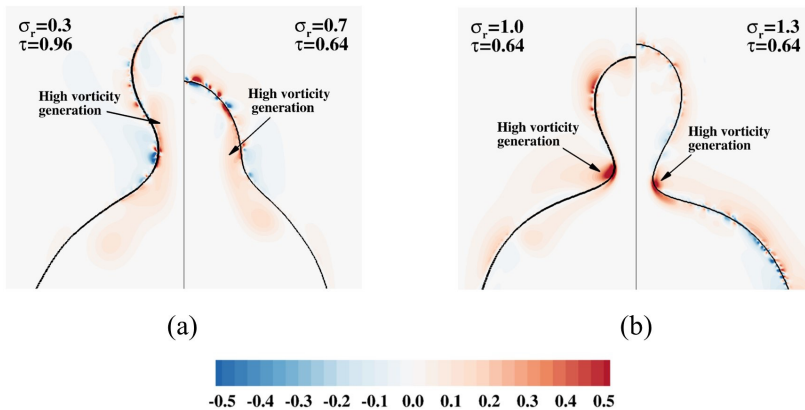


FIG. 11. Comparison of vorticity field contours (normalized by maximum vorticity value) for four different cases of σ_r : (a) left panel for $\sigma_r = 0.3$ and right panel for $\sigma_r = 0.7$, and (b) left panel for $\sigma_r = 1.0$ and right panel for $\sigma_r = 1.3$. The other parameters are $D_r = 2.1$ and $Oh = 0.0035$.

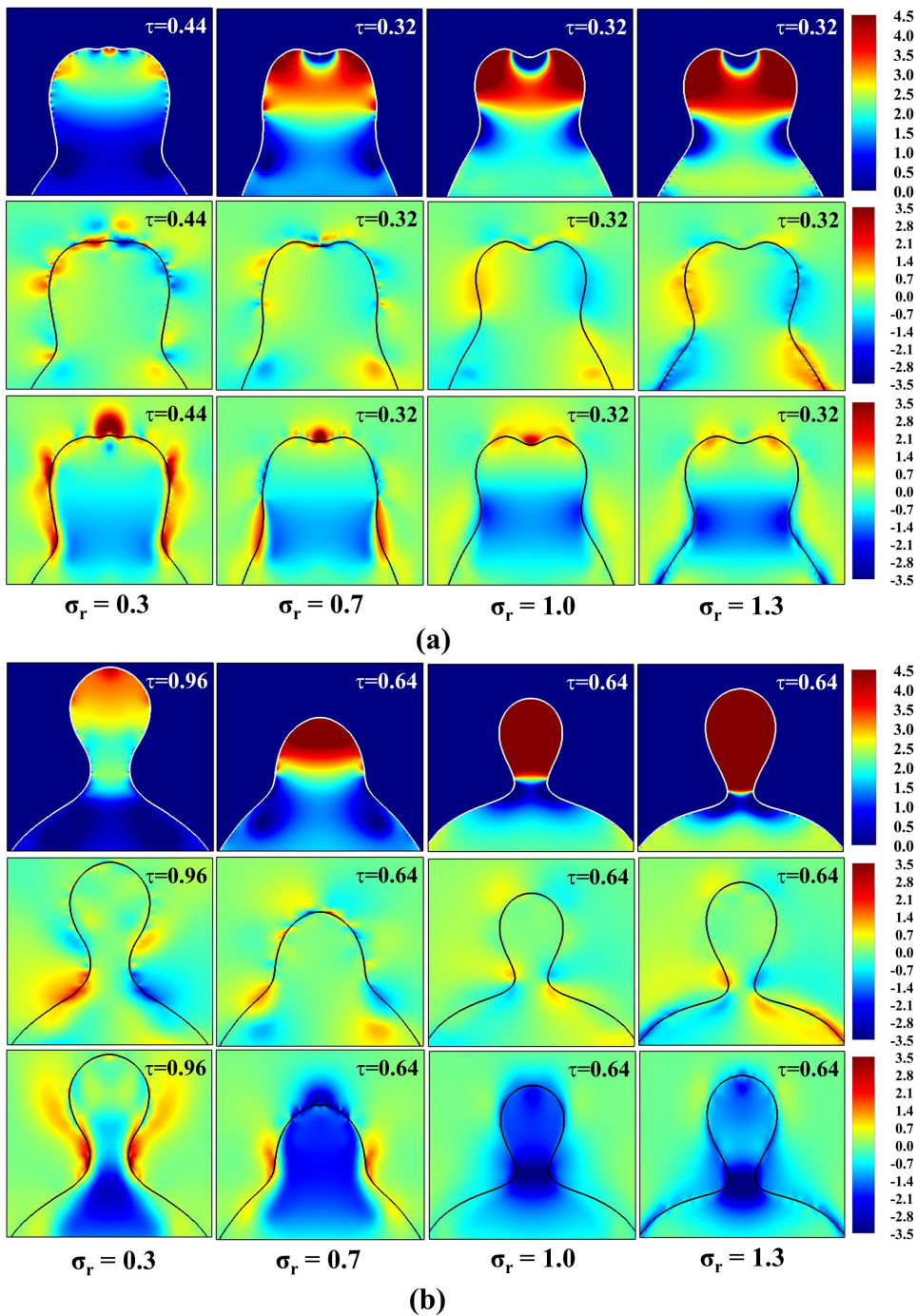


FIG. 12. Comparison of pressure (top row), radial velocity (middle row), and vertical velocity (bottom row) contours for four different cases of σ_r at two distinct time steps: (a) $\tau = 0.32$ for $\sigma_r = 0.7, 1.0,$ and 1.3 and $\tau = 0.44$ for $\sigma_r = 0.3$, and (b) $\tau = 0.64$ for $\sigma_r = 0.7, 1.0,$ and 1.3 and $\tau = 0.96$ for $\sigma_r = 0.3$. Top row: the pressure. The simulations are performed under following parameters: $D_r = 2.1$ and $Oh = 0.0035$.

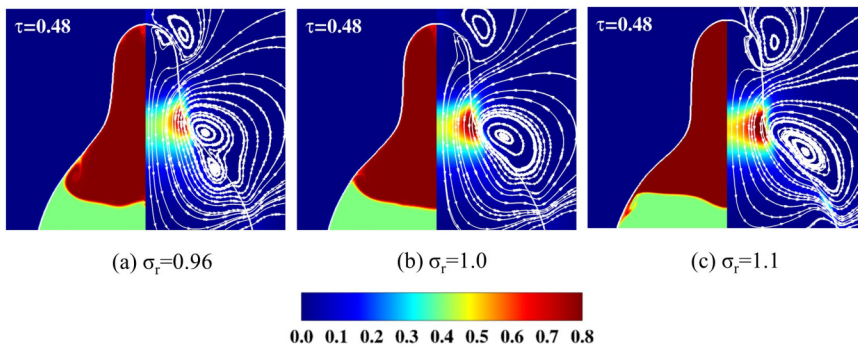


FIG. 13. A zoomed view of interface shape (left panel: the volume fraction, F_1 and right panel: the kinetic energy field normalized by maximum value) superimposed with streamlines showing the tangential motion generated due to mismatched surface tension for (a) $\sigma_r = 0.96$, (b) $\sigma_r = 1.0$, and (c) $\sigma_r = 1.1$. The upper drop, lower drop and the surrounding air in left panel is shown by red, green and blue color, respectively. The legend in figure is given for the kinetic energy field. The other simulation parameters are $D_r = 2.1$ and $Oh = 0.0035$.

to the intense Marangoni stresses, the increase in liquid column height is found to be highest for $\sigma_r = 0.3$ (at $\tau = 0.96$) than for other σ_r . In comparison to the cases corresponding to $\sigma_r = 1.0$ and 1.3 , the case with $\sigma_r = 0.7$ case exhibits a high pressure zone near the tip of the drop at $\tau = 0.32$ that increases the downward motion of the upper drop liquid, resulting in no pinch-off. In addition, the vertical rate of momentum is observed to be higher for the $\sigma_r = 0.7$ instance at $\tau = 0.64$ when compared to other cases.

It is important to note that the main difference between the various σ_r is the tangential stresses occurring along the interface. As previously stated, the tangential flow takes place when liquids with different surface tensions come in contact, causing the lower surface tension liquid to spread over the higher surface tension liquid. A close-up view of the interface shown by volume fraction (F_1) contour (left panel) and the kinetic energy contour (right panel) superimposed with streamlines is shown in Fig. 13 to compare the tangential motion of different σ_r at the region where the upper and lower drop liquids meet. The lower drop and the surrounding fluid are presented in distinct colours for better presentation (green and blue color, respectively). The direction of tangential motions are found to be inward when $\sigma_r < 1.0$, however, the motions are outward in direction when $\sigma_r > 1.0$ as illustrated in Fig. 13 (see also radial and vertical velocity contours from Fig. 12). Also, as seen in Fig. 7(a), the kinetic energy increases as the σ_r grows. The kinetic energy contours shown in Fig. 13 exhibit similar behavior.

The second-stage pinch-off happens at the critical boundary of the first-stage pinch-off and no pinch-off. It is observed that the principal curvatures of the neck during retraction play a key role in the formation of secondary drops. In Fig. 14, the dynamics of second-stage pinch-off is examined. For two different values of σ_r (0.98 and 1.1) that have different pinch-off scenarios, Fig. 14(a) displays a close-up view of neck forms at the commencement of pinch-off. The other dimensionless parameters used for the simulation are as follows: $Oh = 0.005$ and $D_r = 2.1$. In the case of $\sigma_r = 1.1$, the neck is able to close at the initial contact point and pinches off to form secondary droplets. Nevertheless, the thin neck grows again without generating a secondary drop in the case of $\sigma_r = 0.98$. The axial curvature (κ_x) is sharper in the case of $\sigma_r = 0.98$, as shown in the neck profiles.

The method of fitting inscribed circles is used to calculate the value of axial curvature (κ_x) [44]. In this method, a circle with a radius equal to the local radius of curvature in the neck region is fitted into the interface shape as shown in Fig. 14(b). The curvatures at the onset of the first-stage and the second-stage pinch-off are compared in Figs. 14(b) and 14(c), respectively. The curvatures are plotted from the moment a neck formed at the base of the liquid column up to the commencement of pinch-off. The curvatures for first-stage pinch-off are shown in the time range, $\tau = 0.52$ to 0.80 for

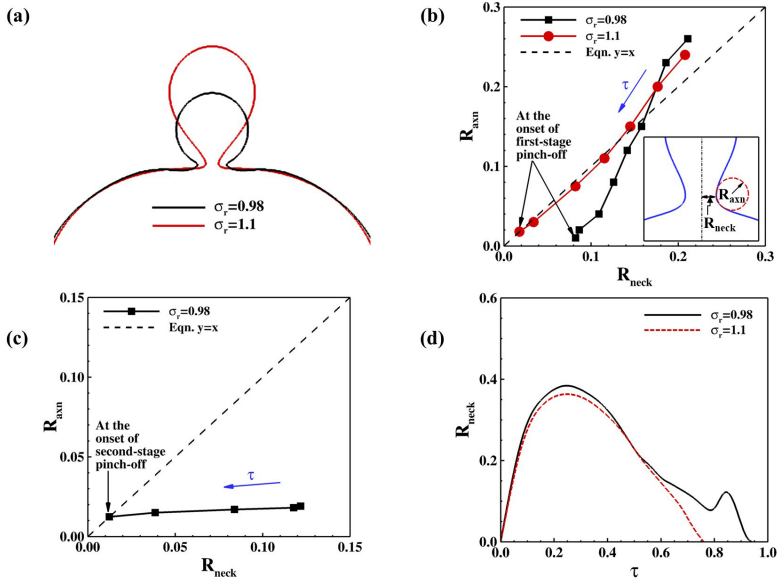


FIG. 14. (a) A close-up view of neck shape. (b) Variation of R_{axn} with R_{neck} for first-stage pinch-off with the curvatures plotted in time range, $\tau = 0.52$ to 0.74 and $\tau = 0.52$ to 0.80 for $\sigma_r = 1.1$ and 0.98 , respectively. (c) Variation of R_{axn} with R_{neck} for second-stage pinch-off with the curvatures plotted in time range, $\tau = 0.84$ to 0.92 for $\sigma_r = 0.98$, and (d) temporal variation of R_{neck} for $\sigma_r = 0.98$ and 1.1 . The other relevant parameters are $D_r = 2.1$ and $Oh = 0.005$.

$\sigma_r = 0.98$ curve and $\tau = 0.52$ to 0.74 for $\sigma_r = 1.1$ curve. The curvatures for second-stage pinch-off are shown in the time range, $\tau = 0.84$ to 0.92 for $\sigma_r = 0.98$. For the first-stage pinch-off, the two principal curvatures (κ_x and κ_θ) at the onset of pinch-off are nearly identical in the case of $\sigma_r = 1.1$, whereas in the case of $\sigma_r = 0.98$, the value of axial curvature, κ_x , is found to be larger than the azimuthal curvature (κ_θ)

Because the axial curvature is always trying to draw the neck back while the azimuthal curvature is trying to squeeze the neck, further neck merging and pinch-off are prevented for $\sigma_r = 0.98$ cases as a result of $\kappa_x > \kappa_\theta$. In other words, since the two principal curvatures are opposite in sign, the capillary pressure that causes motion $\sigma(\kappa_\theta - \kappa_x)$ changes sign, causing a growing neck, which leads to the secondary drop formation in the second stage of coalescence. However, there is no evidence of capillary driven pressure in the case of $\sigma_r = 1.1$. Therefore, the secondary drop pinch-off occurs in the first step of the coalescence cascade. In the case of $\sigma_r = 1.1$, the equality of two principle curvatures for smaller values of R_{neck} may also be seen from equation $y = x$, which is indicated by dashed lines [see Fig. 14(b)]. The comparison of two main curvatures at the commencement of second-stage pinch-off in the case of $\sigma_r = 0.98$ is presented in Fig. 14(c). It is evident that for $\sigma_r = 0.98$, the azimuthal curvature gets substantially sharper in the second stage of coalescence, resulting in the pinch-off of a secondary drop in the second stage.

The transition to the second-stage pinch-off can also be explained by the drainage of the upper drop into the bulk liquid. The temporal variation of neck radius (R_{neck}) for two different values of σ_r (0.98 and 1.1) is shown in Fig. 14(d). For $\sigma_r = 1.1$, the upper drop continues to drain into the bulk liquid. This draining pulls the neck down, making it thinner and allowing the pinch-off to take place. However, in the case of $\sigma_r = 0.98$, the drainage rate decreases, preventing the neck from moving downward. As a result, the axial curvature at the neck increases, causing the neck to expand and the second stage of the coalescence cascade to begin. The neck radius oscillates only once with time for

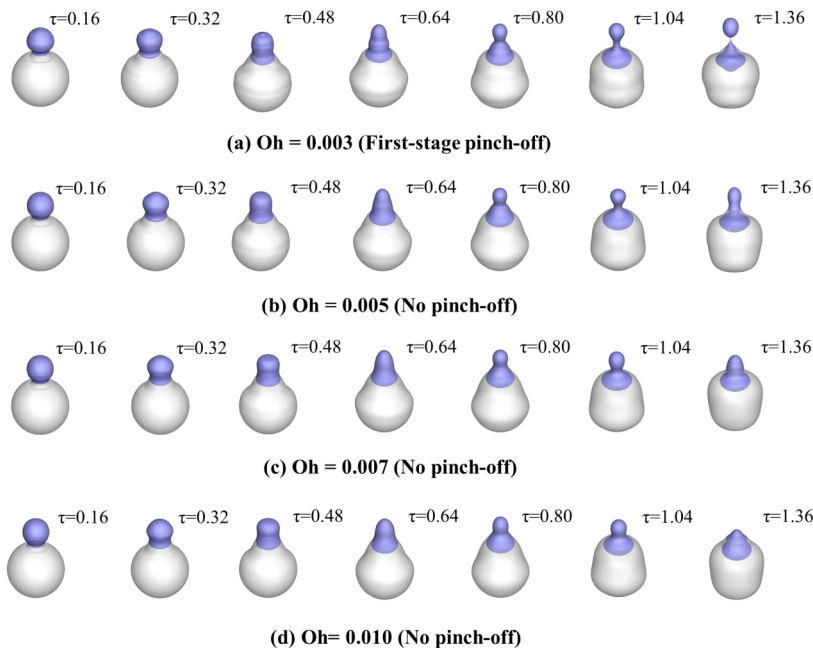


FIG. 15. Distinct pinch-off regimes obtained during the coalescence of two drops for $\sigma_r = 0.3$ and $D_r = 2.1$ at varying Ohnesorge number. To better visualise the coalescence process, a 3D view of 2D axisymmetric results is shown above.

$\sigma_r = 1.1$, however, for $\sigma_r = 0.98$, the number of oscillations grows to two due to neck expansion, indicating that the pinch-off occurs in the second stage of coalescence.

B. Effect of Ohnesorge number

To illustrate the influence of Oh on partial coalescence at a large surface tension difference, we showed four different coalescence scenarios corresponding to increasing Oh in Fig. 15. The other nondimensional parameters are set to $\sigma_r = 0.3$ and $D_r = 2.1$. A constant surface tension ratio ($\sigma_r = 0.3$) means that for all Oh, the upper drop is made of water and lower drop is made of ethanol. This also implies that the Ohnesorge number (defined as $Oh = \mu_1 / \sqrt{\rho_1 \sigma_1 D_u}$) is only varied by changing the upper drop diameter, D_u keeping other parameters constant. When the Oh falls below a particular value, partial coalescence occurs [Fig. 15(a)]; however, as Oh rises over that value, the upper droplet is entirely merged within the bulk liquid, as shown for Figs. 15(b)–15(d). At a lower Oh ($Oh = 0.003$), when a neck forms between two liquid drop interface with different surface tensions, it expands rapidly and generates a strong Marangoni flow that propagates quickly up to the upper drop apex. The liquid from the upper drop starts to drain into the lower drop. The Marangoni flow that reaches the apex of the drop sets a strong converging flow that pulls the drop vertically upward and causes it to deform into a columnar structure. Due to the downward capillary pressure gradient, the apex of the upper drop gathers during vertical stretching, deforming into a bulb shape, while the ligament underneath is elongated vertically. As the bulb expands, Rayleigh-Plateau instability causes the neck to break up, resulting in the secondary droplet. When the Oh is increased to $Oh = 0.005$, the Marangoni flow becomes less intense, resulting in a reduction in both drop deformation and lifting motion. The viscous force dampens the Marangoni flow as the Oh grows. It is also observed that the Marangoni flow becomes substantially weaker at a larger Oh and hence, the lifting motion of the upper drop is barely visible ($Oh = 0.01$). As a result, rather than being prolonged as in Fig. 15(a), the vertical rate of collapse accelerates, and the neck widens before it

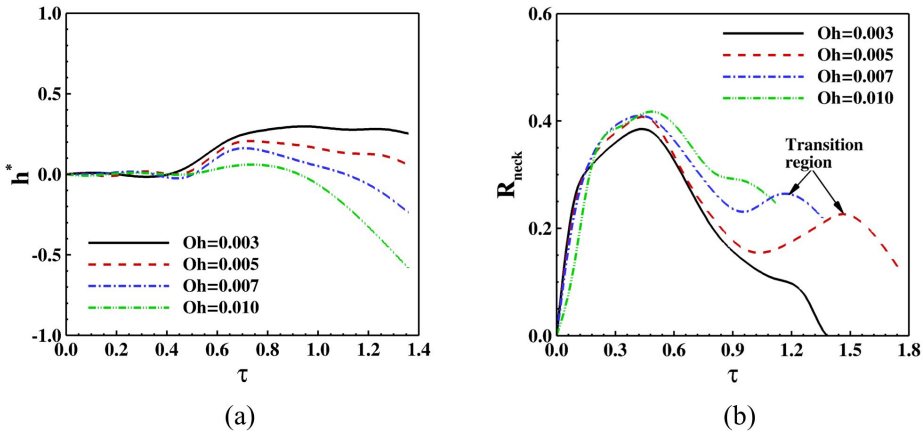


FIG. 16. Effect of Ohnesorge number on temporal evolution of (a) h^* and (b) R_{neck} . The other nondimensional parameters are set to $\sigma_r = 0.3$ and $D_r = 2.1$.

can develop a large capillary force in the inward direction to assist pinch-off. It is also visible from the figure that the vortex ring pattern that arises at $\text{Oh} = 0.003$, no longer exists as the Oh increases, and a bulge type pattern appears at a higher Oh such as $\text{Oh} = 0.01$.

Figure 16 reports the impact of increased Oh on the temporal evolution of the relative upper drop apex height (h^*) and the neck radius (R_{neck}). The other dimensionless parameters remain the same as that of Fig. 15. During the initial stage of coalescence ($\tau < 0.45$), the increased Oh has no effect on the droplet apex height (h^*). However, after $\tau > 0.45$, the vertical stretching of the upper drop is suppressed as the Oh is increased. This is mostly owing to large viscous forces, which result in significant damping of Marangoni stresses as Oh values increase. It is clearly visible in Fig. 14(a) that the maximum value of h^* is significantly lowered at high Oh and the drop collapses rapidly into the lower drop. Furthermore, large Oh causes more neck area spreading, resulting in the highest value of neck radius at $\text{Oh} = 0.01$, as shown in Fig. 16(b).

The temporal variation of the neck radius (R_{neck}) also reveals the transition from first-stage pinch-off to no pinch-off. The neck radius oscillates only once with time and subsequently decreases to zero in the first-stage pinch-off ($\text{Oh} = 0.003$). However, when Oh is increased beyond $\text{Oh} = 0.003$, the transition to no pinch-off happens for $\text{Oh} = 0.005$ and 0.007 cases, where the upper drop oscillates twice before being fully absorbed into the lower drop. When the value of Oh is increased further ($\text{Oh} = 0.01$), the number of oscillations is reduced to one again. At a high Oh , the contact period of the upper drop with the lower drop surface also rises, resulting in a minor shift of curves to the right. It is also clearly seen from the figure that as the Oh increases from 0.005 to 0.01, the total time required for the upper drop to entirely engulfed in the bulk liquid decreases significantly.

The trends in Fig. 16(a) are reflected in Fig. 17 that shows the temporal dynamics of the different energies. The energies are calculated and normalized in the same manner as described earlier in the discussion of Fig. 7. The behavior of kinetic energy is almost identical at all Oh , with an initial increase followed by a decrease. However, with increasing Oh , the kinetic energy reduces, as obvious from Fig. 17(a). In addition, for high Oh , the oscillations in the combined drop shape cause a slight increase in kinetic energy at later time instants ($\tau > 0.9$) when the two drops are combined into single drop. The primary reason for the decrease in kinetic energy with increasing Oh is that the development of the neck is delayed due to the high viscous forces. Even before the necking begins, a considerable percentage of the kinetic energy is wasted, and the pinch-off is hindered due to a lack of energy. The contact area between the two liquid droplets continues to expand until the upper drop is immersed in the lower drop. As a result, no pinch-off phenomenon is visible. This explains why the kinetic energy decreases when Oh increases. Since the total energy of the system at initial time

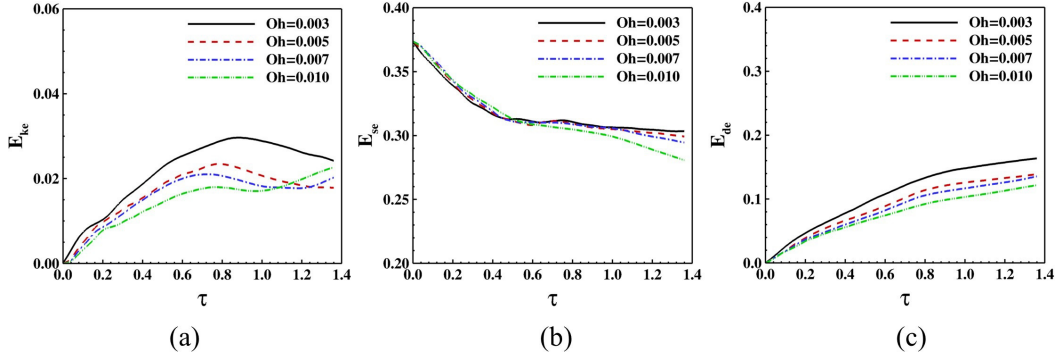


FIG. 17. Effect of Ohnesorge number on temporal evolution of (a) the kinetic energy (E_{ke}), (b) the surface energy (E_{se}), and (c) the dissipation energy (E_{de}) for $\sigma_r = 0.3$ and $D_r = 2.1$.

step is composed primarily of the surface energy of two drops, the initial surface energy is the same for all Oh cases with a constant σ_r ($\sigma_r = 0.3$). As time progresses, the surface energy is converted into kinetic energy and then eventually dissipated by the effects of viscosity. When two drops begin to coalesce, the surface energy initially increases until $\tau < 0.5$ and then declines as Oh grow [see Fig. 17(b)]. One may also observe an increase in dissipation energy when the Oh reduces, as shown in Fig. 17(c). This is because the dissipation energy is only dependent on the Ohnesorge number and velocity components [see Eqs. (16) and (17)]. Nevertheless, as shown in Fig. 17(a), the kinetic energy for lower Oh is considerably greater than that for higher Oh. This indicates that velocity components have a substantial effect on the various energies. Therefore, the dissipation energy is slightly higher at lower Oh. Furthermore, the difference in dissipation energy between various Oh is found to be significantly less than the difference in kinetic energy, owing to the effect of Oh [see Eq. (17)].

The dependence of r_d and τ_p on the Oh for contrast pinch-off scenarios over a wide range of σ_r ($0.3 \leq \sigma_r \leq 1.6$) is plotted in Figs. 18(a) and 18(b). The value of D_r is set to 2.1. The graph shows that there is a considerable amount of variation in the size of secondary droplets and the pinch-off time for both first and second-stage pinch-off. For a particular Oh, the size of secondary

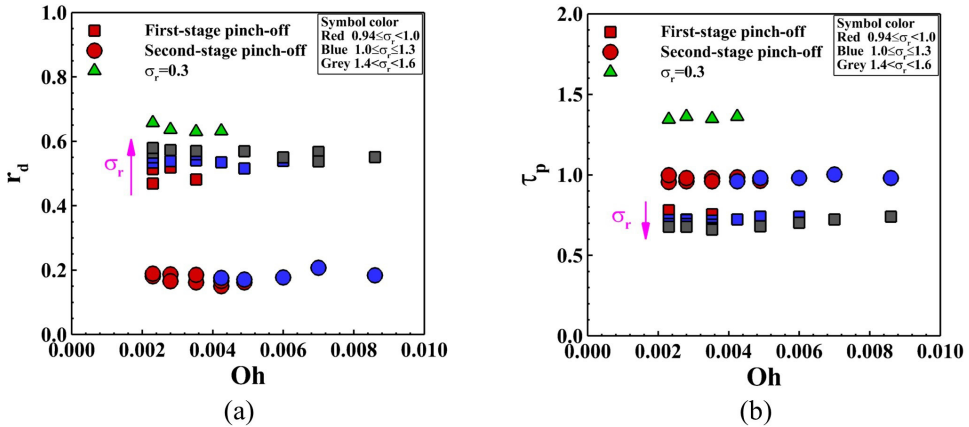


FIG. 18. (a) Effect of Ohnesorge number on secondary drop size ratio (r_d) showing different pinch-off regimes and (b) pinch-off time (τ_p) versus Oh for varying σ_r . The diameter ratio of two drops is fixed as $D_r = 2.1$.

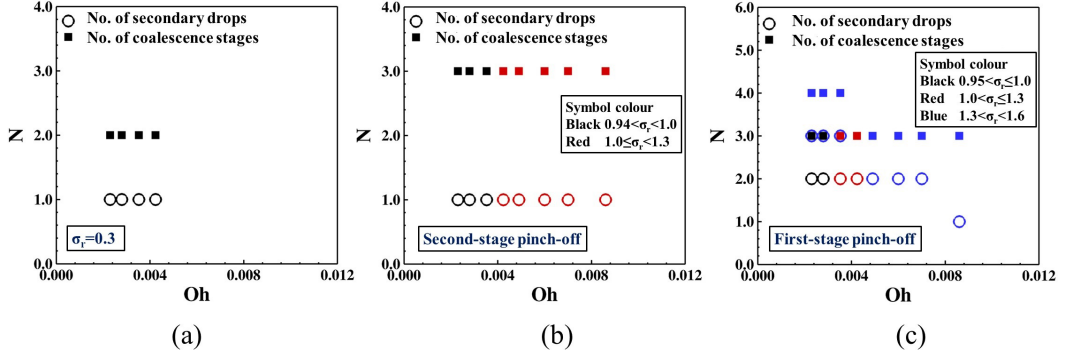


FIG. 19. Effect of Ohnesorge number on total number of coalescence stages and generated secondary drops for three different conditions over a wide range of surface tension ratio (σ_r): (a) $\sigma_r = 0.3$, (b) second-stage pinch-off, and (c) first-stage pinch-off for a fixed $D_r = 2.1$.

drop (r_d) increases with an increase in σ_r [see arrow in Fig. 18(a)], both for first and the second-stage pinch-off, as we have also seen in Fig. 8(a). However, the average value at each stage for the first- and second-stage pinch-off appears to be nearly invariant in terms of Oh. Previous studies [22,23] suggest that the second-stage pinch-off occurs predictably at the first-stage pinch-off-to-no pinch-off boundary. In addition, it is anticipated that only large droplets will produce pinch-off in the second stage or pinch-off in the first stage, as extremely small droplets do not cause pinch-off in the second stage due to the large Oh.

According to earlier studies [22,23,47], the critical range of Oh for the second-stage pinch-off to occur is between 0.004 and 0.01. Furthermore, Chen *et al.* [19] reported that the partial coalescence primarily occurs in the inertial-capillary regime range ($0.004 \leq \text{Oh} \leq 0.01$ and $0.01 \leq \text{Bo} \leq 0.1$). It is clearly shown in the figure that the second-stage pinch-off regime in the current simulation only occurs at the value of $\text{Oh} < 0.01$ (within the inertial-capillary regime). The size of secondary drops for $\sigma_r = 0.3$ is found to be slightly reduced with an increase in the Oh owing to high viscous forces.

With an increase in the Oh, the pinch-off time increases by a small amount for $\sigma_r = 0.3$. For a given Oh, the pinch-off time for the first-stage as well as second-stage pinch-off reduces continuously as the σ_r rises, similar to Fig. 8(b) [see arrow in Fig. 18(b)]. However, with variation in the Oh values, the average value of pinch-off time for the creation of secondary drops is found to be almost constant and independent of Oh for both the first-stage and the second-stage pinch-off. Zhang *et al.* [22] determines the overall time length for second-stage pinch-off as a function of the time required for first-stage pinch-off:

$$(\tau_p)_s = (\tau_p)_f [1 + (r_d)_f^{1.5}], \quad (19)$$

where τ_{pf} and τ_{ps} indicate the total pinch-off time for the first-stage and second-stage pinch-off, respectively. $(r_d)_f$ represents the secondary drop size ratio for the first-stage pinch-off. Using the range of $(r_d)_f = (0.47-0.58)$ and $(\tau_p)_f = (0.66-0.78)$, the theoretical value of $(\tau_p)_s$ from Eq. (19) ranges between $(0.87-1.12)$, which is nearly identical to the range of $(\tau_p)_s = (0.95-1.0)$ obtained from our numerical data.

For various pinch-off scenarios, Fig. 19 shows the effect of Oh on the total number of secondary drops produced and the total number of coalescence stages that occur during the whole coalescence cascade. The other parameters are the same as shown in Fig. 18. For $\sigma_r = 0.3$ and the second-stage pinch-off regime, the number of secondary drops and coalescence stages appears to be constant and is independent of Oh as visible from Figs. 19(a) and 19(b). For a given Oh, the total number of secondary drops and coalescence stages increases with increasing σ_r in case of first-stage pinch-off as seen in Fig. 19(c). However, as the Oh rises, the number of secondary drops reduces from 4 to 3 and the number of coalescence stages decreases from 3 to 1. This is due to the high viscous forces,

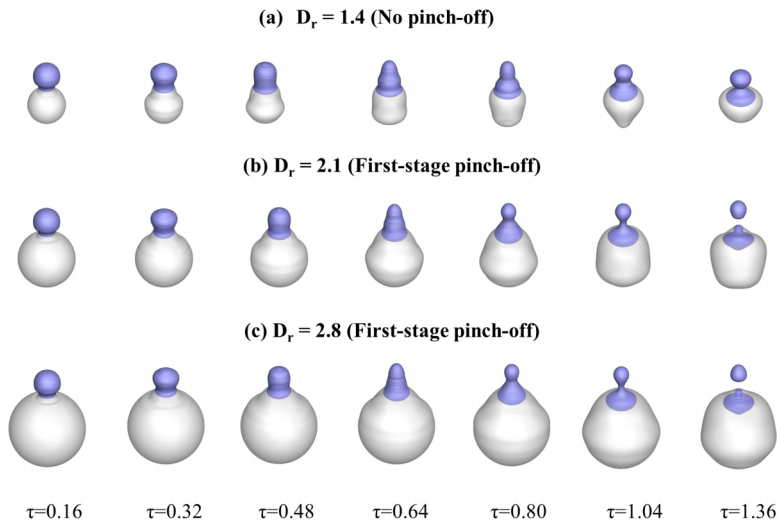


FIG. 20. Distinct pinch-off regimes obtained during the coalescence of two unequal-sized drops for $Oh = 0.0035$ and $\sigma_r = 0.3$ at varying parent drop size ratio (D_r). For a better understanding of the coalescence process, a 3D view of 2D axisymmetric results is displayed above.

which enable the upper drop liquid to drain more quickly as it comes into contact with the lower drop, reducing the number of secondary drops created as well as the number of coalescence stages.

C. Effect of parent drop size ratio

For a large surface tension difference ($\sigma_r = 0.3$), Fig. 20 analyzes the coalescence phenomenon at varying D_r . The Oh is fixed at 0.0035. According to previous studies [48,49], the coalescence of two equal-sized drops always results in no pinch-off and the pinch-off occurs only when the size ratio is greater than one. The minimum D_r over which a secondary drop pinches off, according to Zhang *et al.* [22] experimental observations, is around 1.55. Blanchette and Bigioni [49] suggested this value to be 1.6 based on the numerical simulations. As shown in Fig. 20, even in the presence of strong Marangoni forces, no pinch-off occurs at a lower D_r , $D_r = 1.4$. For large D_r , such as 2.1 and 2.8, a first-stage pinch-off occurs. The reason for this behavior is that although the Marangoni flow causes sufficient stretching and lifting motion to the upper drop at a smaller D_r , the lower drop is also deformed and stretched in the same way as the upper drop due to convergence of capillary waves at the apex of the lower drop. It is also observed in previous studies (Deka *et al.* [24]) that during the coalescence of two drops, the capillary pull convergence on the lower drop apex limits the neck inward movement and prevents the secondary drop pinch-off.

Figure 20 also shows that the deformation and stretching in the lower drop surface reduces, when the D_r increases. This occurs because of the fact that the capillary waves must cover a longer distance to reach the bottom surface of the lower drop in the case of bigger lower drops. Furthermore, as the propagation of the capillary wave is continuously attenuated by the viscous forces, the intensity of the capillary waves reduces, resulting in a decreased downward capillary force. Consequently, at large D_r , the neck closes before the capillary waves hit the bottom of the lower drop surface, resulting in the neck pinch-off. Blanchette and Bigioni [49] also indicated that during the coalescence of two drops, the surface tension of the lower drop causes an extra downward force of magnitude, σ_2/R_l (R_l being the lower drop radius), which tries to draw the upper drop towards its center. This downward force works in the same way as the gravitational force, increasing the amount of drainage from the upper drop. In addition, Fig. 20 demonstrates that the vortex ring pattern appears when the D_r is significant, but it is absent when the D_r is lower.

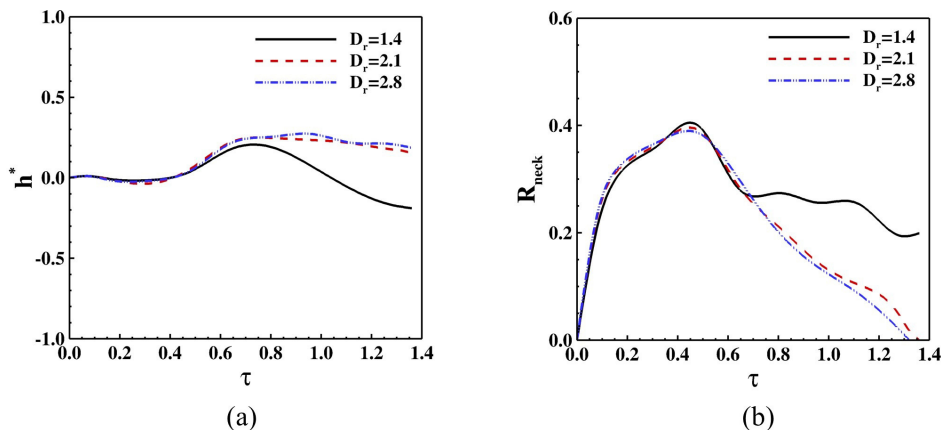


FIG. 21. Effect of parent drop size ratio on temporal evolution of (a) h^* and (b) R_{neck} . The other nondimensional parameters are fixed to $\sigma_r = 0.3$ and $\text{Oh} = 0.0035$.

To further demonstrate the effect of Marangoni flow on the D_r , Fig. 21 illustrates the temporal evolution of upper drop apex height (h^*) and neck radius (R_{neck}). The simulation conditions are identical to those given in Fig. 20. In comparison to the other D_r cases, the overall apex height of upper drop at lower D_r ($D_r = 1.4$) is observed to be smaller owing to the capillary wave convergence at lower drop apex, as discussed in Fig. 20. Increasing the D_r from 2.1 to 2.8 has little effect on the vertical elongation as shown in Fig. 21(a). The variation of neck radius in Fig. 21(b) shows that for $D_r = 2.1$ or 2.8, the neck radius decreases rapidly after reaching a maximum due to an increase in the inward movement of the pinching neck, resulting in the creation of secondary drops. However, for $D_r = 1.4$, the neck radius grows slightly after reaching maximum as a result of the reopening of the neck caused by an insufficient inward horizontal momentum rate. Therefore, when the drop diameter ratio is small ($D_r = 1.4$), the neck expands more than in other situations. In addition, the highest value of neck radius (R_{neck}) is found to be nearly same in all three cases.

The effect of D_r on the temporal evolution of different energies is reported in Fig. 22. It is important to note that in all three cases, the energies are calculated using Eqs. (14)–(16), and are normalized by the initial surface energy for drops of $D_r = 2.1$ with no surface tension gradients. The figure shows that for a fixed Oh and σ_r , the larger the D_r , the higher the surface energy and kinetic energy. However, for large D_r values, the kinetic energy increases until the neck pinches off, then

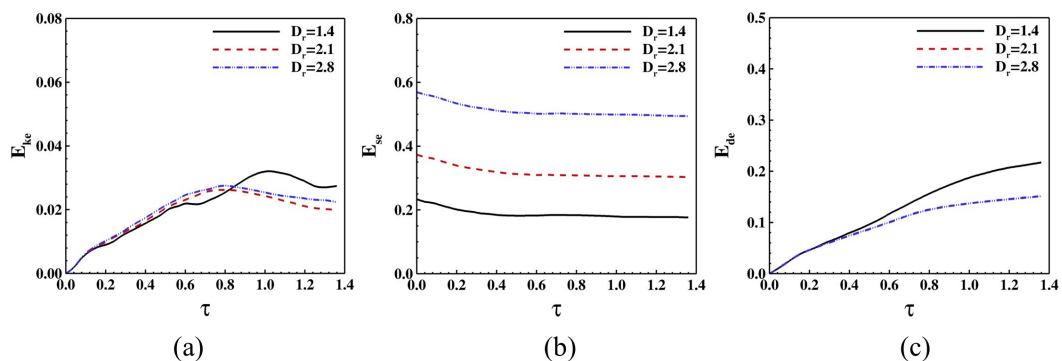


FIG. 22. Effect of parent drop size ratio (D_r) on temporal evolution of (a) the kinetic energy (E_{ke}), (b) the surface energy (E_{se}), and (c) the dissipation energy (E_{de}) for $\text{Oh} = 0.0035$ and $\sigma_r = 0.3$.

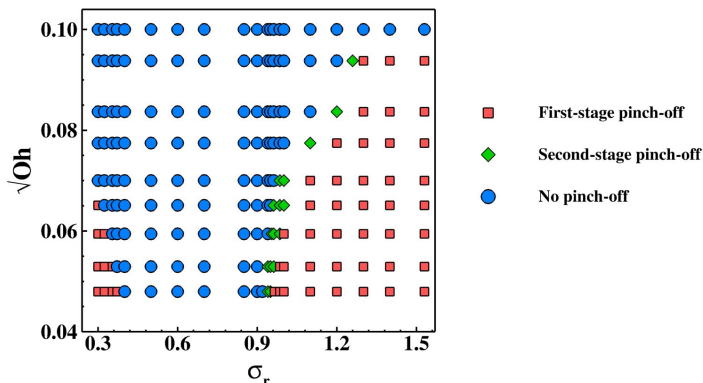


FIG. 23. Different pinch-off regimes identified during coalescence of two miscible drops in Oh- σ_r plane for $D_r = 2.1$.

reduces quickly due to the separation of secondary drops [see Figs. 22(a) and 22(b)]. Additionally, at the initiation of pinch-off ($\tau = 0.6$ – 0.8), the kinetic energy for $D_r = 1.4$ is observed to be reduced, while the dissipation energy increases as compared to $D_r = 2.1$ and 2.8 , indicating the insufficient kinetic energy for the generation of secondary drop in case of $D_r = 1.4$ [see Fig. 22(c)].

D. Regime map

Finally, a regime map on the Oh- σ_r plane is drawn in Fig. 23 for size ratio, $D_r = 2.1$, to highlight the distinct outcomes achieved during the coalescence of two unequal-sized droplets with different σ_r . The coalescence of two miscible drops gives three different outcomes: no pinch-off, first-stage pinch-off, and second-stage pinch-off. The nonmonotonic behavior of the coalescence process is clearly visible in Fig. 23, which shows partial coalescence emergence at $\sigma_r > 0.9$ for $Oh < 0.01$, disappearance at $0.4 < \sigma_r < 0.94$ for all Oh, and reappearance at lower σ_r for $Oh < 0.005$. The second-stage pinch-off happens for all Oh values except when $Oh = 0.01$ between the first-stage pinch-off and no pinch-off regimes. At a higher value of Oh ($\sqrt{Oh} = 0.1$), there is no pinch-off regime regardless of the σ_r . As capillary wave propagation is suppressed by the high viscous forces at large Oh, the value of critical σ_r , above which a secondary drop pinches off, is observed to monotonically increase with an increase in Oh. Blanchette *et al.* [26] reported that the smallest value of σ_r beyond which no pinch-off regime occurs is 0.93 at lower strength of viscous and gravity force for the case of a drop coalescing into a flat liquid pool. In the current study, the smallest value of critical σ_r below which no secondary drops are formed is 0.94 for $Oh = 0.0023$ and $Bo = 0.0$.

V. CONCLUSIONS

In the present study, the pinch-off dynamics of two unequal-sized drops made of dissimilar but miscible liquids is explored using the CLSVOF method. The critical behavior of the unbalanced surface tension forces and viscous forces on the partial coalescence process has been addressed. The significance of parent drop size ratio on the re-emergence of partial coalescence in the presence of a high surface tension differential between two drops is discussed. The main points drawn in the current study based on the current numerical work are explained below:

(i) Depending on the σ_r , the presence of surface tension gradients along the interface between two unequal-sized drops results in a nonmonotonic behavior of partial coalescence consisting of emergence, disappearance, and re-emergence. During the coalescence process, there are three distinct pinch-off regimes: first-stage, second-stage, and no pinch-off.

(ii) When $\sigma_r > 1.0$, the tangential motion generated by the difference in surface tension has a little influence on the coalescence process. The conditions under which the upper drops with higher surface tension encounter partial coalescence, however, are considerably constrained when $\sigma_r < 1.0$

due to the intrusive movement of the lower drop fluid. The converging surface flow that occurs for $\sigma_r < 1.0$ facilitates the detachment of the vortex ring produced during two drops coalescence from the interface surface.

(iii) Over a wide range of σ_r , the size of secondary drops and the pinch-off time for both first- and second-stage pinch-off are found to be nearly independent of the Oh. Large viscous forces inhibited the propagation of tangential motions and favored total coalescence even at a high surface tension difference between two drops ($\sigma_r = 0.3$). A transition regime develops between partial and total coalescence at $\sigma_r = 0.3$ with an increase in the Oh. Furthermore, the secondary drop pinch-off at a large surface tension differential is also prevented for smaller D_r .

(iv) After a large number of simulations, a regime map for the distinct coalescence outcomes on the Oh- σ_r plane is presented. The critical σ_r increases monotonically with increasing Oh due to the suppression of capillary waves by significant viscous forces at higher Oh values. In our simulation, the minimum value of σ_r required for partial coalescence to occur is 0.94 at low values of the Ohnesorge and Bond numbers (Oh = 0.0023 and Bo = 0.0).

ACKNOWLEDGMENT

The authors thank the Indian Institute of Technology Kanpur and the Ministry of Education, Government of India under the IMPRINT initiative for providing the High Performance Computational facility to carry out the simulations.

-
- [1] J. J. Thomson and H. F. Newall, V. On the formation of vortex rings by drops falling into liquids, and some allied phenomena, *Proc. R. Soc. Lond.* **39**, 417 (1886).
 - [2] A. V. Anilkumar, C. P. Lee, and T. G. Wang, Surface tension induced mixing following coalescence of initially stationary drops, *Phys. Fluids A* **3**, 2587 (1991).
 - [3] S. Singh and A. K. Saha, Numerical study of heat transfer during oblique impact of a cold drop on a heated liquid film, *J. Thermal Sci. Eng. Appl.* **15**, 050907 (2023).
 - [4] E. X. Berry and R. L. Reinhardt, Analysis of cloud drop growth by collection. 3. Accretion and self-collection, *J. Atmos. Sci.* **31**, 2118 (1974).
 - [5] E. Villermaux, Fragmentation, *Annu. Rev. Fluid Mech.* **39**, 419 (2007).
 - [6] A. Bhakta and E. Ruckenstein, Decay of standing foams: Drainage, coalescence and collapse, *Adv. Colloid Interface Sci.* **70**, 1 (1997).
 - [7] H. Stone, A. Stroock, and A. Ajdari, Engineering flows in small devices: Microfluidics toward a lab-on-a-chip, *Annu. Rev. Fluid Mech.* **36**, 381 (2004).
 - [8] K. Sun, P. Zhang, Z. Che, and T. Wang, Marangoni-flow-induced partial coalescence of a droplet on a liquid/air interface, *Phys. Rev. Fluids* **3**, 023602 (2018).
 - [9] S. T. Thoroddsen and K. Takehara, The coalescence cascade of a drop, *Phys. Fluids* **12**, 1265 (2000).
 - [10] F. Blanchette and T. P. Bigioni, Partial coalescence of drops at liquid interfaces, *Nat. Phys.* **2**, 254 (2006).
 - [11] G. E. Charles and S. G. Mason, The coalescence of liquid drops with flat liquid/liquid interfaces, *J. Colloid Sci.* **15**, 236 (1960).
 - [12] H. Yang, C. C. Park, Y. T. Hu, and L. G. Leal, The coalescence of two equal-sized drops in a two-dimensional linear flow, *Phys. Fluids* **13**, 1087 (2001).
 - [13] A. Ramachandran and L. G. Leal, Effect of interfacial slip on the thin film drainage time for two equal-sized, surfactant-free drops undergoing a head-on collision: A scaling analysis, *Phys. Rev. Fluids* **1**, 064204 (2016).
 - [14] G. D. M. Mackay and S. G. Mason, The gravity approach and coalescence of fluid drops at liquid interfaces, *Can. J. Chem. Eng.* **41**, 203 (1963).
 - [15] J. Eggers, J. R. Lister, and H. A. Stone, Coalescence of liquid drops, *J. Fluid Mech.* **401**, 293 (1999).

-
- [16] J. D. Paulsen, J. C. Burton, and S. R. Nagel, Viscous to Inertial Crossover in Liquid Drop Coalescence, *Phys. Rev. Lett.* **106**, 114501 (2011).
- [17] C. R. Anthony, P. M. Kamat, S. S. Thete, J. P. Munro, J. R. Lister, M. T. Harris, and O. A. Basaran, Scaling laws and dynamics of bubble coalescence, *Phys. Rev. Fluids* **2**, 083601 (2017).
- [18] C. Constante-Amores, A. Batchvarov, L. Kahouadji, S. Shin, J. Chergui, D. Juric, and O. Matar, Role of surfactant-induced Marangoni stresses in drop-interface coalescence, *J. Fluid Mech.* **925**, A15 (2021).
- [19] X. Chen, S. Mandre, and J. J. Feng, Partial coalescence between a drop and a liquid-liquid interface, *Phys. Fluids* **18**, 051705 (2006).
- [20] T. Gilet, K. Mulleners, J. P. Lecomte, N. Vandewalle, and S. Dorbolo, Critical parameters for the partial coalescence of a droplet, *Phys. Rev. E* **75**, 036303 (2007).
- [21] B. Ray, G. Biswas, and A. Sharma, Generation of secondary droplets in coalescence of a drop at a liquid-liquid interface, *J. Fluid Mech.* **655**, 72 (2010).
- [22] F. H. Zhang, E. Q. Li, and S. T. Thoroddsen, Satellite Formation During Coalescence of Unequal-Size Drops, *Phys. Rev. Lett.* **102**, 104502 (2009).
- [23] H. Ding, E. Q. Li, F. H. Zhang, Y. Sui, P. D. M. Spelt, and S. T. Thoroddsen, Propagation of capillary waves and ejection of small droplets in rapid droplet spreading, *J. Fluid Mech.* **697**, 92 (2012).
- [24] H. Deka, G. Biswas, S. Chakraborty, and A. Dalal, Coalescence dynamics of unequal-sized drops, *Phys. Fluids* **31**, 012105 (2019).
- [25] H. P. Kavehpour, Coalescence of drops, *Annu. Rev. Fluid Mech.* **47**, 245 (2015).
- [26] F. Blanchette, L. Messio, and J. W. M. Bush, The influence of surface tension gradients on drop coalescence, *Phys. Fluids* **21**, 072107 (2009).
- [27] Blanchette, Simulation of Mixing Within Drops due to Surface Tension Variations, *Phys. Rev. Lett.* **105**, 074501 (2010).
- [28] A. H. Saifi and M. K. Tripathi, Distinct coalescence behaviors of hot and cold drops in the presence of a surrounding viscous liquid, *Phys. Fluids* **32**, 082101 (2020).
- [29] D. W. Martin and F. Blanchette, Simulations of surfactant effects on the dynamics of coalescing drops and bubbles, *Phys. Fluids* **27**, 012103 (2015).
- [30] T. Dong, W. H. Weheliye, and P. Angeli, Laser induced fluorescence studies on the distribution of surfactants during drop/interface coalescence, *Phys. Fluids* **31**, 012106 (2019).
- [31] H. Manikantan and T. M. Squires, Surfactant dynamics: Hidden variables controlling fluid flows, *J. Fluid Mech.* **892**, P1 (2020).
- [32] S. Shim and H. A. Stone, Damped coalescence cascade of liquid drops, *Phys. Rev. Fluids* **2**, 044001 (2017).
- [33] I. S. Khattab, F. S. Bandarkar, M. A. A. Fakhree, and A. Jouyban, Density, viscosity, and surface tension of water+ethanol mixtures from 293 to 323k, *Korean J. Chem. Engineering* **29**, 812 (2012).
- [34] J. U. Brackbill, D. B. Kothe, and C. Zemach, A continuum method for modeling surface tension, *J. Comput. Phys.* **100**, 335 (1992).
- [35] S. Osher and J. A. Sethian, Fronts propagating with curvature dependent speed, *J. Comput. Phys.* **79**, 12 (1988).
- [36] K. Sun, F. Jia, P. Zhang, L. Shu, T. Wang *et al.*, Marangoni Effect in Bipropellant Droplet Mixing During Hypergolic Ignition, *Phys. Rev. Appl.* **15**, 034076 (2021).
- [37] D. Gueyffier, J. Li, A. Nadim, S. Scardovelli, and S. Zaleski, Volume of fluid interface tracking with smoothed surface stress methods for three-dimensional flows, *J. Comput. Phys.* **152**, 423 (1999).
- [38] M. Sussman and E. G. Puckett, A coupled level set and volume-of-fluid method for computing 3D and axisymmetric incompressible two-phase flows, *J. Comput. Phys.* **162**, 301 (2000).
- [39] G. Son and N. Hur, A coupled level set and volume-of-fluid method for the buoyancy-driven motion of fluid particles, *Numer. Heat Transfer, Part B* **42**, 523 (2002).
- [40] G. Son, Efficient implementation of a coupled level-set and volume-of-fluid method for three-dimensional incompressible two-phase flows, *Numer. Heat Transfer, Part B* **43**, 549 (2003).
- [41] Z. Wang, J. Yang, B. Koo, and F. Stern, A coupled level set and volume-of-fluid method for sharp interface simulation of plunging breaking waves, *Int. J. Multiphase Flow* **35**, 227 (2009).

- [42] S. Singh and A. K. Saha, Numerical study of flow and heat transfer during a high-speed micro-drop impact on thin liquid films, *Int. J. Heat Fluid Flow* **89**, 108808 (2021).
- [43] S. Singh and A. K. Saha, Dynamics of two unequal-sized drops coalescence at a liquid-liquid interface, *Phys. Fluids* **34**, 063604 (2022).
- [44] S. T. Thoroddsen, K. Takehara, and T. G. Etoh, The coalescence speed of a pendent and a sessile drop, *J. Fluid Mech.* **527**, 85 (2005).
- [45] R. B. J. Koldewej, B. F. van Capelleveen, D. Lohse, and C. W. Visser, Marangoni-driven spreading of miscible liquids in the binary pendant drop geometry, *Soft Matter* **15**, 8525 (2019).
- [46] F. H. Zhang, M.-J. Thoraval, S. T. Thoroddsen, and P. Taborek, Partial coalescence from bubbles to drops, *J. Fluid Mech.* **782**, 209 (2015).
- [47] A. A. Alhareth and S. T. Thoroddsen, Partial coalescence of a drop on a larger-viscosity pool, *Phys. Fluids* **32**, 122115 (2020).
- [48] A. Menchaca-Rocha, A. Martínez-Dávalos, R. Núñez, S. Popinet, and S. Zaleski, Coalescence of liquid drops by surface tension, *Phys. Rev. E* **63**, 046309 (2001).
- [49] F. Blanchette and T. P. Bigioni, Dynamics of drop coalescence at fluid interfaces, *J. Fluid Mech.* **620**, 333 (2009).